991

UNIVERSITE DE NEUCHATEL

INSTITUT DE MICROTECHNIQUE

ELASTIC AND PHOTOELASTIC PROPERTIES OF SINGLE-MODE OPTICAL FIBERS: APPLICATION TO THE MEASUREMENT OF FORCE

THESE

PRESENTEE A LA FACULTE DES SCIENCES

POUR OBTENIR LE GRADE DE DOCTEUR ES SCIENCES

PAR

Axel Bertholds

Neuchâtel, le 26 septembre 1986

IMPRIMATUR POUR LA THÈSE

Propriétés élastiques et photo-élastiques des fibres optiques monomode: application à la mesure des forces

de Monsieur Axel Bertholds

UNIVERSITÉ DE NEUCHATEL

FACULTÉ DES SCIENCES

La Faculté des sciences de l'Université de Neuchâtel, sur le rapport des membres du jury,

Messieurs R. Dändliker, N. de Rooij, Ph. Robert (EPF-Lausanne) et H.R. Zulliger (Greifensee)

autorise l'impression de la présente thèse.

Neuchâtel, le 20 janvier 1987

Le doyen:

François Sigrist

Les tirés à part ci-joints représentent l'essentiel de la thèse de doctorat dont le titre et le nom de l'auteur sont repris en page de garde.
Le texte complet du manuscrit peut être consulté à la bibliothèque de l'Institut de Microtechnique, rue A.-L. Breguet 2, 2000 Neuchâtel.

Liste de publications

- R. Dändliker, A. Bertholds, "Microprocessor based phase determination for high resolution optical sensors", Proc. Journées d'Electronique 1984 (Presses Polytechniques Romandes, Lausanne, 1984), pp. 239-245.

- A. Bertholds, R. Dändliker, "Microprocessor based phase determination for high resolution optical sensors", Electronics Lett., vol. 21, pp. 65-67, 1985.

- A. Bertholds, R. Dändliker, "High resolution photoelastic pressure sensor using low-birefringence fiber", Appl. Opt., vol. 25, pp. 340-343, 1986.

- A. Bertholds, R. Dändliker, "Deformation of single-mode optical fibers under static longitudinal stress", accepted for publication in IEEE Journ. of Lightwave Techn. 1987.

- A. Bertholds, R. Dändliker, "Determination of the individual strain-optic coefficients in single-mode optical fibers", accepted for publication in IEEE Journ. of Lightwave Techn., 1987.

Reprinted from Proc. of Journées d'Electronique 1984
(Presses Polytechniques Romandes, Lausanne, 1984).

MICROPROCESSOR BASED PHASE DETERMINATION FOR HIGH RESOLUTION OPTICAL SENSORS

R. Dändliker and A. Bertholds
Institut de Microtechnique de l'Université
CH-2000 Neuchâtel, Switzerland

Summary

Interferometric and polarimetric sensors are traditionally limited by their non-linear input-output characteristics. To get high resolution and high sensitivity, it is necessary to count the periods of the output signals and interpolate their phase accurately. A microprocessor controlled phase measuring system for high resolution sensors is described. An automatic calibration procedure provides drift compensation and long-term accuracy. Interpolation with a resolution of 1/1000 of a fringe is demonstrated experimentally.

Résumé

Les senseurs interférométriques et polarimétriques sont traditionnellement limités par leurs caractéristiques entrée-sortie non-linéaires. Afin d'obtenir une haute résolution et une haute sensibilité, il est nécessaire de compter les périodes des signaux de sortie et d'interpoler leur phase avec précision. Un système de mesure de phase commandé par microprocesseur, destiné à des senseurs à haute précision, est décrit. Un cycle automatique de calibrage fournit une compensation des dérives et une précision à long terme. Une interpolation résolvant 1/1000 de frange est demontrée expérimentalement.

Introduction

In the field of metrology by optical interferometry, it is often necessary to measure the induced phase changes between two coherent light beams with high resolution. For instance, in the case of interferometric sensors [1,2], resolutions of more than 10^4 points are often desired. In general, the superposition of the interference beams appears as a pattern of fringes which, projected onto photodetectors, creates sinusoidal electrical signals as a function of the phase difference. Therefore, to get high resolution and high sensitivity from these periodic signals, it is necessary to count the running fringes as well as to interpolate their position accurately.

A typical example is the Michelson interferometer shown in Fig.1.a, where a displacement of the movable mirror by half a wavelength produces at the output a shift of one fringe. By illuminating two suitably placed photodetectors within the fringe pattern, two electrical signals in quadrature (90° phase-shift) can be obtained. This is necessary for bi-directional fringe counting and allows fringe interpolation with phase independent accuracy. Further, to eliminate the effect of intensity fluctuations, an additional reference detector is employed to monitor the total intensity. This is realized, for instance, by using a large detecting surface, integrating over several fringes.

Fig.1.

Interferometric and polarimetric sensors:
a) Michelson interferometer

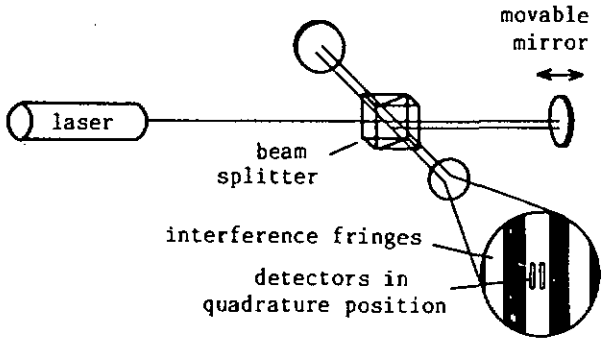

b) fiber sensor measuring force induced birefringence.

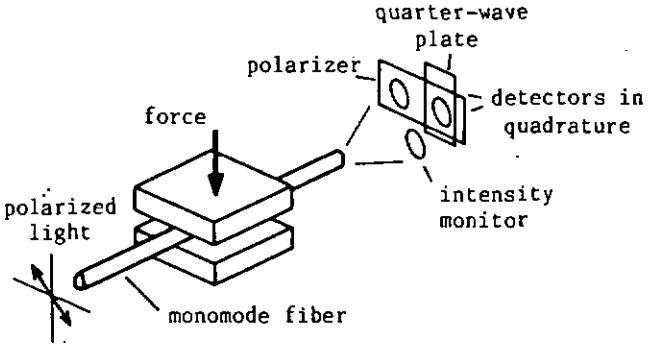

Another important class of optical sensors are the polarimetric sensors [2,3], which do not exhibit at the output a fringe pattern but from which two quadrature signals can be obtained by placing appropriate optical elements (polarizers, optical retarders) in front of the photodetectors. An example is shown in Fig.1.b, where the birefringence induced in a single-mode optical fiber by a transverse force is measured [3]. The linear polarization of the input light and the linear polarizer in front of two of the detectors are orientated at 45° with respect to the direction of the applied force. The quarter-wave plate supplies the 90° phase-shift and a third detector at the output of the fiber serves as intensity monitor.

Phase determination

In general, the problem of counting and interpolating interference fringes can be solved by heterodyne techniques [4] with phase and time independent resolution of better than 1° (~1/300 of a fringe). However, this analog approach requires sophisticated optical components and electronics (optical modulators, phasemeters), making it less attractive for most sensor applications.

An alternative solution is to employ the two signals in quadrature from the detectors mentioned above. In practice, these signals as a function of the interference phase ϕ are given by

$$I_1 = a_1 [1 + m_1 \cos(\phi)] , \quad (1)$$

$$I_2 = a_2 [1 + m_2 \cos(\phi - \psi)] , \quad (2)$$

where a_1 and a_2 are the DC-levels, m_1 and m_2 the modulation depths and ψ is the relative phase-shift of about 90°. To determine the interference phase

accurately, the exact values of these parameters have to be known or to be controlled. Traditionally, they are adjusted to predetermined values ($a_1 = a_2$, $m_1 = m_2$, $\psi = 90°$) by means of optical alignment and electrical adjustment. However, these parameters may change with time due to thermal effects, mechanical and optical misalignment, electronical drift, etc., thus limiting the long-term accuracy usually desired in sensor applications. The influence of the most likely and most rapid changes, namely the intensity fluctuations (source power fluctuations, sensor losses), is eliminated immediately by normalizing the signals I_1 and I_2 to the reference intensity I_r.

The present work reports on a microprocessor based approach to the problem, which has the advantage that all hardware adjustments, electronical, optical and mechanical, are replaced by adaption of numerical parameters in software. The microprocessor calculates the value of the interference phase from the simultaneously detected and A/D converted signal levels I_1, I_2 and I_r, using the relation

$$\tan \phi = (\{m_1[(I_2/a_2 I_r) - 1]/m_2[(I_1/a_1 I_r) - 1]\} - \cos \psi)/\sin \psi. \qquad (3)$$

Through a calibration procedure, the actual values of the parameters a_i, m_i and ψ, which are assumed to change only slowly, are automatically determined, stored, and updated from time to time. Finally, the number of periods counted (by means of a bi-directional counter) and the interpolated phase are appropriately added to get the total accumulated phase.

It is worth noticing here the reasons why Eq.(3) is used to calculate the phase. First, the obtained accuracy is phase independent, and secondly, the effect of common variations of the modulation depths (reduction of coherence, optical misalignment, etc.) is eliminated by the presence of the ratio m_1/m_2 only.

Microprocessor controlled system

The phase measuring system consists of three separate blocks (see Fig.2), namely the fast bi-directional counter for the number of periods, the sampler and A/D converter for the interpolation, and the acquisition procedure for the calibration. The task of the microprocessor is to control these three operations as well as to perform the calculations involved.

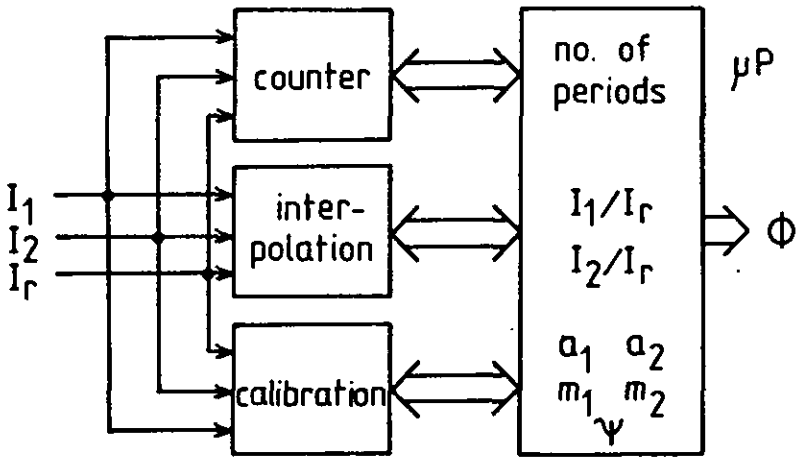

Fig.2.

Block diagram of the phase measuring system.

While the quadrature signals vary periodically with the interference phase, their time behaviour may look quite different, depending essentially on how the physical parameter to be measured is converted into an optical phase change. An example is given in Fig.3, where the detector signal at the output of a loaded and unloaded fiber optic force sensor (Fig.1.b) is shown as a function of time (0.1 s/div). Obviously, the counter must be designed to be fast enough to follow the periodic signals (typically between some Hz and 100 kHz, depending on the application). Since high frequency and low amplitude phase fluctuations may be present, a digital hysteresis must be included to assure a correct bi-directional counting.

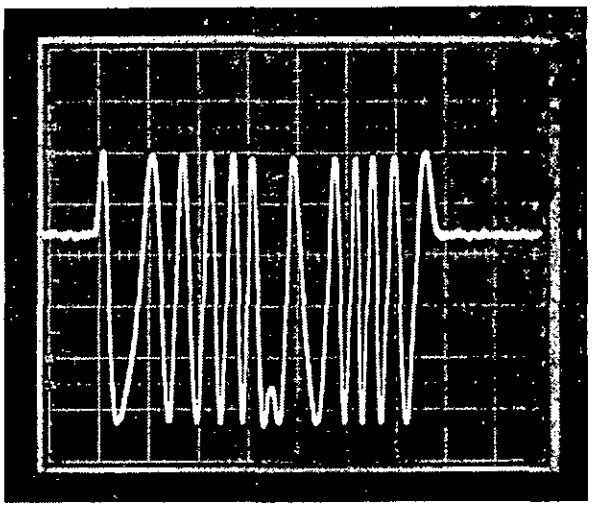

Fig.3.

Time behaviour of a detector signal at the output of a loaded and unloaded fiber optic sensor (0.1 s/div).

To determine accurately the interference phase from the detected signal levels, it is important to sample them simultaneously. The number of required bits for the A/D conversion depends on the desired precision. For example, using Eq.(3) with the ideal values of the calibration parameters ($m_1 = m_2 = 1$, $\psi = 90°$), 8 bits are required for a phase resolution of about 1°. As explained earlier, the values of the parameters a_i, m_i and ψ, which may vary with time, are determined by a calibration procedure. The overall precision of the phase measurement system depends therefore on how accurate their values are calculated and on how frequently the calibration is performed.

To calculate these parameters, the values of the three output signals I_1, I_2 and I_r, are sampled simultaneously at six particular positions within the same period. These positions should not differ too much from the six ideal positions shown in Fig.4, as will be explained later. Depending on the time behaviour of the signals, this can be done either by hardware, synchronizing the sampling at the desired positions (by means of zero-crossing and level comparator circuits) or by software, sampling a great number of values and then selecting the six ones which fit best the desired positions.

Note that, to enable this sampling procedure, the signals at the output of a sensor must exhibit phase changes of at least one period, preferably during a short time interval to assure accuracy. Fortunately, this is what usually happens in most sensor applications, where, during normal operation, several periods are passed through. If this is not the case, a phase modulator may be added for this purpose.

Calculating the calibration parameters

Six of the 18 sampled values are intensity references (see Fig.4). They are used to normalize the values of the other two detectors, as usual. The resulting 12 values, namely

$$I_{1n} = a_1 [\ 1 + m_1 \cos(\phi_n)]\ ,$$
$$I_{2n} = a_2 [\ 1 + m_2 \cos(\phi_n - \psi)]\ , \qquad (n = 1,2,\ldots,6) \qquad (4)$$

form a set of 12 equations with 6 unknown phases ϕ_n corresponding to the exact positions of the samples and the 5 calibration parameters to be determined, totalizing 11 unknown parameters. This set of equations is solved by means of iteration, using an algorithm which benefits of the fact that the approximate values of the phases ϕ_n are known, namely the 6 ideal positions shown in Fig.4, corresponding to 0°, 45°, 90°, 180°, 225° and 270°.

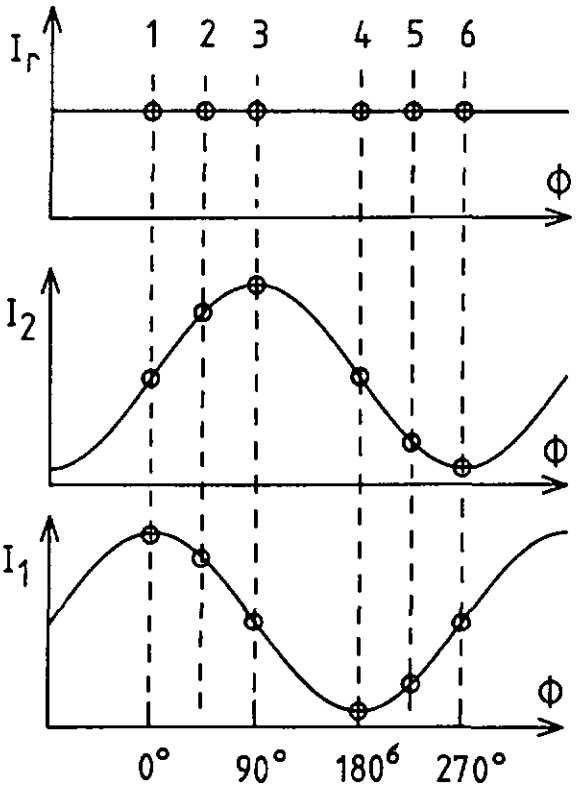

Fig.4.

Output signals as a function of phase ϕ, with the (ideal) sampling positions numbered from 1 to 6.

First, one assumes that all the samples were taken at the ideal positions, and that the two signals were exactly in quadrature, that is $\psi = 90°$. From the values of I_{11}, I_{14}, I_{23} and I_{26} (which are quite insensitive to the phase of the signals), one calculates a first approximation of a_1, a_2, m_1 and m_2. Using these approximations and the values of I_{13}, I_{16}, I_{21} and I_{24} (which are most sensitive to the phase of the signal), the phases ϕ_1, ϕ_3, ϕ_4 and ϕ_6 are determined. Then, from the samples number 2 and 5, which are sensitive to the relative phase of the signals, one is able to calculate the parameter ψ as well as the remaining phases ϕ_2 and ϕ_5. Once a complete set of first approximations of ϕ_n and ψ is obtained, a second iteration

using these new approximations is performed. Finally, this is continued until the desired accuracy for the five calibration parameters is achieved. The number of necessary iterations will depend, of course, on the differences between the sampled and the ideal positions, and the precision aimed. For phase differences up to ± 10° and for two signals phase-shifted by 90°, a precision of 0.1% is obtained after 8 iterations (worst case). For the more realistic case of $\psi = 90° \pm 5°$, the maximum number of iterations increases to 17.

Experimental setup used to test the phase measuring system

The calibration procedure and the accurate phase interpolation have been tested experimentally by means of the setup shown in Fig.5. The two quadrature signals and the intensity reference are obtained by illuminating three photodetectors with a laser diode emitting linearly polarized light. A polarizer and a quarter-wave plate are suitably placed in front of the detectors, and their outputs are connected to a 12-bit A/D converter controlled by a microcomputer. The phase changes are introduced by placing at the output of the laser a Soleil-Babinet compensator, which can be thought of as a manually operated continuously adjustable optical retardation plate. With the help of this device, a phase change of about two periods can be produced with a resolution of 0.2°.

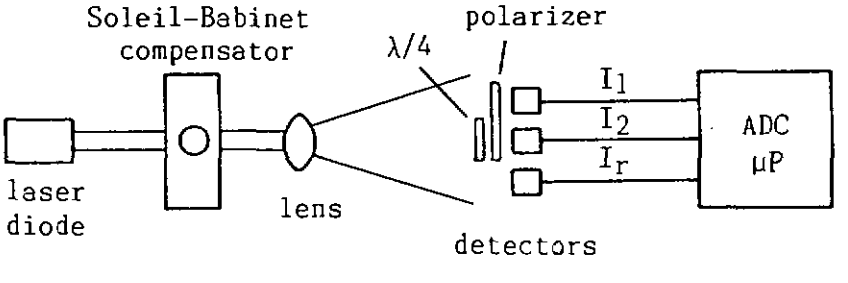

Fig.5. Experimental setup used to test the phase measuring system.

First, the reproducibility of the calibration procedure has been tested. The calibration parameters have been determined by taking the samples at positions with random deviations from the ideal values within ± 10°. For 20 successive determinations, the standard deviations of the resulting parameters were less than 0.1%.

Secondly, the accuracy of the interpolation has been measured. The phase was calculated using Eq.(3) with previously determined calibration parameters and then compared with the linear response of the compensator. The achieved resolution for a total phase change of one period was 0.3°, which corresponds to an interpolation accuracy of 1/1000 of a period. This is also the limit of the accuracy of the compensator.

Conclusions

A microprocessor controlled phase measuring system for interferometric and polarimetric sensors is described, which employs two electrical signals in quadrature and an intensity monitor. It has the advantage, compared to traditional systems, that no accurate optical, mechanical or electrical adjustments are needed. By means of a calibration procedure, the parameters characterizing the input signals are determined and updated from time to time, assuring thus the long-term accuracy. An iterative algorithm to calculate accurately these parameters is described, and has been tested sucessfully.

Finally, the measuring system has been tested experimentally by simulating a polarimetric sensor using an optical Soleil-Babinet compensator. The reproducibility of the calibration procedure and the interpolation accuracy have been measured under different conditions. The results show an overall accuracy for the system corresponding to at least 1/1000 of a period.

References

[1] D. R. Herriott, "Some applications of lasers to interferometry", Progress in Optics,6, 171-209 (1967).

[2] T. G. Giallorenzi, et al., "Optical Fiber Sensor Technology", IEEE J. Quantum El. QE-18, 626-664 (1982).

[3] R. Ulrich," Fiber-Optic Sensors", Proc.Journée d'Electronique 1982 (Presses Polytechniques Romandes, Lausanne, 1982) pp.73-87.

[4] R. Crane, "New developments in Interferometry. V. Interference Phase Measurement", Appl.Opt. 18, 538-542 (1969).

MICROPROCESSOR-BASED PHASE DETERMINATION FOR HIGH-RESOLUTION OPTICAL SENSORS

Indexing terms: Optics, Optical sensors

A microprocessor-controlled phase measuring system for high-resolution optical sensors is described. An automatic calibration procedure provides drift compensation and long-term accuracy. Using a 12 bit A/D convertor, phase interpolation with a resolution of 0·12° (~1/3000 of a period) is demonstrated.

Introduction: Interferometric and polarimetric sensors are traditionally limited by their nonlinear input/output characteristics. Usually, the information at their output appears as a movement of interference fringes which, projected onto photodetectors, creates sinusoidal electrical signals as a function of the interference phase. Therefore, to get high resolution and high sensitivity, it is necessary to count the running fringes as well as to interpolate their position accurately. In general this problem can be solved by heterodyne techniques. However, this analogue approach requires sophisticated optical components and electronics (optical modulators, phasemeters), making it less attractive for sensor applications. An alternative solution is to produce at the output of the sensor two electrical signals in quadrature (90° phase shift), which allows bidirectional fringe counting and fringe interpolation with phase independent accuracy.

In the case of interferometric sensors, as the Michelson interferometer,[1] the two quadrature signals can be obtained by illuminating two suitably placed photodetectors within the interference pattern. To eliminate the effect of light intensity fluctuations, an additional reference detector is usually employed to monitor the total intensity. In the case of polarimetric sensors,[2] similar output signals can be obtained by placing appropriate optical elements (polarisers, optical retarders) in front of the photodetectors.

Phase determination: In practice, the quadrature signals as a function of the interference phase ϕ are given by

$$I_1 = a_1[1 + m_1 \cos(\phi)] \quad (1)$$

$$I_2 = a_2[1 + m_2 \cos(\phi - \psi)] \quad (2)$$

where a_i are the DC levels, m_i the modulation depths, and ψ is the relative phase shift of about 90°. To determine the interference phase accurately, the exact values of these parameters have to be known or to be controlled. Traditionally they are adjusted to predetermined values by means of optical alignment and electrical adjustment. However, these parameters may change with time due to thermal effects, mechanical and optical misalignment, electronic drift etc., thus limiting the long-term accuracy usually desired in sensor applications. The influence of the most likely and most rapid changes, namely the intensity fluctuations (source power fluctuations, sensor losses), is eliminated immediately by normalising the signals I_1 and I_2 to the reference intensity I_r.

The present work reports on a microprocessor-based phase measuring technique which has the advantage that all hardware adjustments, electronic, optical and mechanical, are replaced by adaption of numerical parameters in software.[3] The microprocessor calculates the value of the interference phase ϕ from the simultaneously detected and A/D converted signal levels I_1, I_2 and I_r, using the relation

$$\tan\phi = (\{m_1[(I_2/a_2' I_r) - 1]/m_2[(I_1/a_1' I_r) - 1]\} - \cos\psi)/\sin\psi \quad (3)$$

(where a_i' represents the normalised value of a_i (i.e. a_i/I_r) as determined by the calibration procedure) which provides phase independent accuracy and insensitivity to common variations of the modulation depths. Through a calibration procedure, the actual values of the parameters a_i, m_i and ψ, which are assumed to change only slowly, are automatically determined, stored and updated from time to time. Finally, the number of periods counted (by means of a bidirectional counter) and the interpolated phase are appropriately added to get the total accumulated phase. Thus, the phase measuring system can be described by three separate blocks (see Fig. 1), namely the fast bidirectional counter for the number of periods, the sampler and A/D convertor for the interpolation, and the data acquisition procedure for the calibration. The task of the microprocessor is to control these three operations as well as to perform the calculations involved.

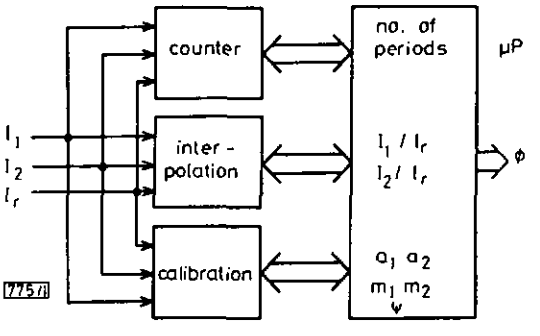

Fig. 1 *Block diagram of the phase measuring system*

The number of required bits for the A/D conversion depends on the desired interpolation accuracy. From eqn. 3 one sees that for typical values of the calibration parameters ($a_1 = a_2$, $m_1 = m_2 = 0{\cdot}9$ and $\psi = 90 \pm 5°$), 8 bits are required to resolve 1/500 of a period and 12 bits for 1/8000 of a period (see Fig. 3). However, the absolute phase accuracy is limited by the accuracy of the employed calibration parameters.

Determination of the calibration parameters: The necessary data for the calibration cycle is obtained by sampling the values of the three output signals I_1, I_2 and I_r simultaneously at six particular positions within the same period. These positions should not differ too much from the six ideal positions shown in Fig. 2, as will be explained later. Depending on the time behaviour of the signals, this can be done either by hardware (synchronising the sampling at the desired positions) or by software (continuous sampling and selection of the six positions which fit best the desired ones). To enable this sampling procedure, the signals at the output of the sensor must exhibit phase changes of at least one period, preferably during a short time interval to assure accuracy. Fortunately, this is what usually happens in most applications, where, during normal operation, several periods are passed through. If this is not the case, a phase modulator may be added for this purpose.

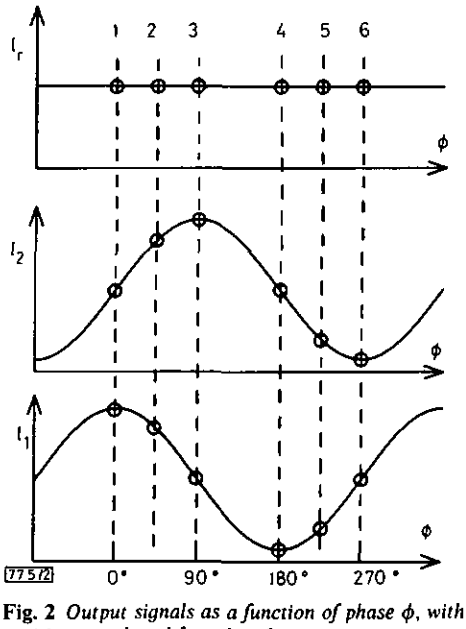

Fig. 2 *Output signals as a function of phase ϕ, with the (ideal) sampling positions numbered from 1 to 6*

Six of the 18 sampled values are intensity references (see Fig. 2) and are used to normalise the values of the other two detectors. The resulting 12 values, namely

$$\left.\begin{aligned} I_{1n} &= a'_1[1 + m_1 \cos(\phi_n)] \\ I_{2n} &= a'_2[1 + m_2 \cos(\phi_n - \psi)] \end{aligned}\right\} \quad n = 1, 2, \ldots, 6 \qquad (4)$$

form a set of 12 equations with six unknown phases ϕ_n corresponding to the exact positions of the samples and the five calibration parameters to be determined, totalling 11 unknown parameters. This set of equations is solved by means of iteration, using an algorithm which benefits from the fact that the approximate values of the phases ϕ_n are known, namely the six ideal positions shown in Fig. 2, corresponding to 0°, 45°, 90°, 180°, 225° and 270°.

First, one assumes that all the samples are taken at the ideal positions, and that the two signals are exactly in quadrature, that is $\psi = 90°$. From the values of I_{11}, I_{14}, I_{23} and I_{26} (which are quite insensitive to the phase of the signals), one calculates a first approximation of a_1, a_2, m_1 and m_2. Using these approximations and the values of I_{13}, I_{16}, I_{21} and I_{24} (which are most sensitive to the phase of the signal), the phases ϕ_1, ϕ_3, ϕ_4 and ϕ_6 are determined. Then, from the samples 2 and 5, which are sensitive to the relative phase of the signals, one is able to calculate the parameter ψ as well as the remaining phases ϕ_2 and ϕ_5. Once a complete set of first approximations of ϕ_n and ψ is obtained, a second iteration using these new approximations is performed. Finally, this is continued until the desired precision for the five calibration parameters is achieved. The number of necessary iterations depends on the precision aimed and on the deviations of the sampled positions from the ideal ones. For example, for deviations up to $\pm 10°$ and for two signals phase shifted by $90 \pm 5°$ (typical case), a precision of 0·1% is obtained after a maximum of 17 iterations. For deviations greater than $\pm 15°$, the algorithm may not always converge.

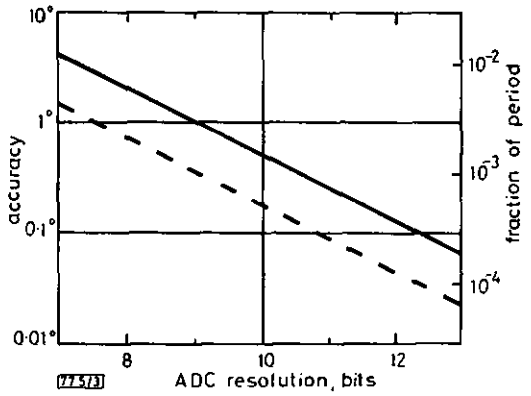

Fig. 3 *Interpolation accuracy as a function of A/D conversion resolution*

Using parameters obtained from one calibration cycle (solid line)
Using exact parameters (broken line)
($a_1 = a_2$; $m_1 = m_2 = 0{\cdot}9$; $\psi = 90 \pm 5°$)

Accuracy of the system: The interpolation accuracy of the system is essentially given by the accuracy of the parameters employed to calculate the phase. For one calibration cycle and for a sufficiently large number of iterations, their accuracy depends on the resolution of the A/D conversion of the input data. This relationship is illustrated in Fig. 3 (solid line). If several calibration cycles are performed, mean values of the parameters can be determined to improve the accuracy towards the ideal case (broken line).

The calibration cycle and the phase interpolation have been tested experimentally by simulating a polarimetric sensor with a Soleil–Babinet compensator.[3] Using a microcomputer controlled 12 bit A/D convertor, an accuracy of 1/1000 of a period has been verified. This corresponds to the limits of the compensator.

A. BERTHOLDS
R. DÄNDLIKER
Institut de Microtechnique
Université de Neuchâtel
CH-2000 Neuchâtel, Switzerland

29th November 1984

References

1 HERRIOTT, O. R.: 'Some applications of lasers to interferometry', *Prog. Opt.*, 1967, **16**, pp. 171–209
2 GIALLORENZI, T. G., *et al.*: 'Optical fiber sensor technology', *IEEE J. Quantum Electron.*, 1982, **QE-18**, pp. 626–664
3 DANDLIKER, R., and BERTHOLDS, A.: 'Microprocessor based phase determination for high resolution optical sensors'. Proceedings of the Journées d'Electronique 1984 (Presses Polytechniques Romandes, Lausanne, 1984), pp. 239–245

Reprinted from Applied Optics, Vol. 25, page 340, February 1, 1986

High-resolution photoelastic pressure sensor using low-birefringence fiber

A. Bertholds and R. Dändliker

The effect of birefringence induced in a single-mode fiber by a lateral force has been applied to measure the absolute value of force or pressure with high resolution. A sensor configuration with an extended detecting surface has been investigated by means of calibrated weights. The sensor is sensitive to an incremental force of 2×10^{-3} N, independently of the length of the fiber. The maximum force applied was 10 N/m of fiber length.

I. Introduction

When a single-mode fiber is pressed between parallel plates, birefringence is introduced due to an asymmetrical transverse stress distribution induced in the core region.[1] By measuring the change of polarization of the light propagating through the fiber, the applied force can be determined. In this paper, the application of this effect to measure the absolute value of static force or pressure with high resolution and accuracy is investigated.

Squeezing a single-mode fiber laterally over a short length (~1 cm) with either a small static force[2] or a periodic force[3] has proved to be a simple and practical way of transforming the state of polarization of light passing through the fiber. Also, measurement of the birefringence induced in a coiled single-mode fiber by an acoustic wave has been used as a polarimetric acoustic sensor.[4] However, to the best of our knowledge, the effect of birefringence induced in single-mode fibers by a lateral force has not been applied yet to measure the absolute value of static force or pressure. Several fiber-optic pressure sensors based on multimode fiber technology have been reported in the literature. Examples are the microbending sensor,[5] where the fiber itself is used as the sensing element, and the photoelastic pressure sensor,[6] where the fibers act as lightguide to and from a bulk sensing element. The present approach uses a single-mode fiber both to guide the light and detect the force. The flexibility of the fiber and the fact that the stress-induced birefringence is integrated along its length enable the construction of sensor configurations with extended detecting surfaces. As a result of the small cross section of the fiber, relatively large stresses are induced in the core region yielding high sensitivity.

II. Sensor Configuration

The sensing element consists of an uncoated low-birefringence single-mode fiber pressed between parallel plates (see Fig. 1). Linearly polarized monochromatic light, aligned at 45° with respect to the direction of the force, is injected into the fiber, thus exiting two polarization modes (parallel and perpendicular to the force, respectively) with equal intensities. At the output end of the fiber, two photodetectors are placed behind appropriate polarization-optical elements. They produce two electrical signals in quadrature (90° phase shift), which vary sinusoidally as a function of the induced birefringence. An additional reference detector serves as monitor for the output light intensity.

This sensor configuration can be viewed as a differential interferometer, where the two light beams travel within the same fiber but with orthogonal polarizations. The change of the fiber birefringence due to the applied force is measured by observing the interference between the two polarization modes. The interference is observed by placing in front of two detectors a polarizer aligned at 45° with respect to the direction of the force. The phase shift of 90° is obtained by introducing a quarterwave plate aligned with its fast axis either parallel or perpendicular to the force, placed between the fiber end and the polarizer in front of one of the detectors (see Fig. 1).

The authors are with Université de Neuchâtel, Institut de Microtechnique, CH-2000 Neuchâtel, Switzerland.
Received 18 July 1985.
0003-6935/86/030340-04$02.00/0.

III. Phase Measuring System

The two signals in quadrature and the intensity reference signal are fed to a microprocessor-controlled phase measuring system which counts the number of periods and interpolates the phase accurately.[7] Compared to traditional analog techniques, this measuring system has the advantage that all hardware adjustments, electronic, optical, and mechanical, are replaced by adaption of numerical parameters in software. After normalization to the intensity reference, the two periodic signals have the form

$$I_1 = a_1[1 + m_1 \cos(\phi)], \tag{1}$$

$$I_2 = a_2[1 + m_2 \cos(\phi - \psi)] \tag{2}$$

where ϕ denotes the phase difference between the two polarization modes, a_i are the dc levels, m_i the modulation depths, and ψ the relative phase shift of ~90°. The change of birefringence is determined from the total number of periods counted and from the interpolated phase, calculated from the relation

$$\tan\phi = (\{m_1[(I_2/a_2) - 1]/m_2[(I_1/a_1) - 1]\} - \cos\psi)/\sin\psi. \tag{3}$$

The accuracy of this phase interpolation is independent of the value of the phase and is insensitive to common variations of the modulation depths m_1 and m_2. To provide drift compensation and long-term accuracy, the measuring system determines and updates the values of the five parameters a_i, m_i, and ψ from time to time by means of a calibration procedure,[7] which benefits from the fact that typically more than one period is passed through when the sensor is actuated. The accuracy of the system is essentially determined by the resolution of the analog-to-digital (A/D) conversion of the input signals. For example, 12-bit A/D conversion is necessary to resolve 1/3000 of a period. Because of the periodic nature of the input signals, the dynamic range of the system is only limited by the capacity of the electronic counter. Since the response of the fiber to an applied force is instantaneous, the measuring bandwidth of the system is mainly limited by the time required for sampling and data processing.

In general, the phase measuring technique described above is suited for applications where the input signals pass through several periods over the range to be measured and where a reproducible readout with a linearity of better than 0.1% is desired. Compared to conventional optical compensator techniques based on electromagnetic or piezoelectric transducers, this technique has the advantage that all the problems associated with the transducer (nonlinear response, hysteresis effects, limited dynamic range) are eliminated, thus enabling high linearity over an unlimited dynamic range.

IV. Induced Birefringence

The birefringence or difference in propagation constants between the two polarization modes of the fiber results from the superposition of two effects, namely, the birefringence induced by the lateral compressive force and the bending-induced birefringence.[8] Assuming that the fiber is elastic and mechanically homogeneous, the birefringence induced by a transverse force F is given by[1]

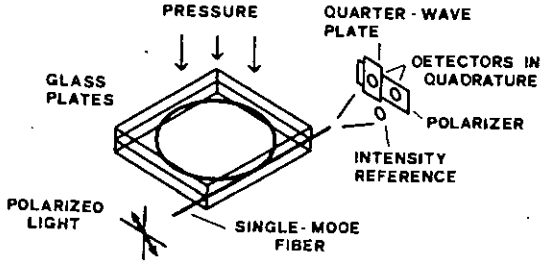

Fig. 1. Sensor configuration.

$$\beta_f = 8Cf/\lambda r, \tag{4}$$

where f is the applied force per unit fiber length (i.e., $f = F/L$, where L is the fiber length), λ is the wavelength, r is the fiber radius, and C is a combination of fiber material parameters, the so-called stress-optic coefficient, given by

$$C = n^3(p_{11} - p_{12})(1 + \nu)/2E, \tag{5}$$

where n is the refractive index of the core region, p_{11} and p_{12} are components of the elastooptic tensor, ν is the Poisson's ratio, and E is the Young's modulus of the fiber material. For fused silica parameters $n = 1.458$, $p_{11} = 0.121$, $p_{12} = 0.270$, $\nu = 0.17$, and $E = 7.3 \times 10^{10}$ N/m^2, the stress-optic coefficient has the value of $C = -3.7 \times 10^{-12}$ m^2/N. For a fiber bend with a radius of curvature R, the induced birefringence is given by[8]

$$\beta_b = \pi CEr^2/\lambda R^2. \tag{6}$$

The fast axis of the force-induced birefringence is parallel to the direction of the applied force, whereas the fast axis of the bending-induced birefringence is perpendicular to the bending axis. For a fiber confined between parallel plates, the bending axis is automatically aligned parallel to the direction of the force. Provided that the fiber has a small intrinsic birefringence and no mechanical twist to produce optical activity,[9] the two contributions to the birefringence have the same principal axes, but their fast axes are perpendicular to each other. Consequently, the resulting birefringence β becomes

$$\beta = \beta_b - \beta_f, \tag{7}$$

where the fast axis ($\beta > 0$) has been arbitrarily chosen to be perpendicular to the direction of the force.

It is important for the accuracy of the sensor that the principal axes of the birefringence are properly aligned parallel and perpendicular to the direction of the applied force. If a low-birefringence fiber is employed (i.e., intrinsic birefringence <10°/m),[10] this alignment will only be perturbed by mechanical twist introduced unvoluntarily when constructing the sensor element. The observed birefringence β_α due to the superposition of β and the optical activity α resulting from the mechanical twist is given by[9]

$$\beta_\alpha = (\beta^2 + \alpha^2)^{1/2} = [\beta^2 + (g\tau)^2]^{1/2}, \quad (8)$$

where τ is the twist rate, and g is the stress-optic rotation coefficient, which has the value of $g = 0.13$ for fused silica fibers.[9] In Fig. 2 the relative error $\delta\beta/\beta = (\beta_\alpha - \beta)\beta$ of the birefringence is plotted as a function of β for different twist rates τ. From this figure one can estimate, for a given accuracy, the amount of mechanical twist which can be tolerated. The same figure shows also that in practice the perturbing effect of the mechanical twist can be eliminated by applying a sufficiently large bias force.

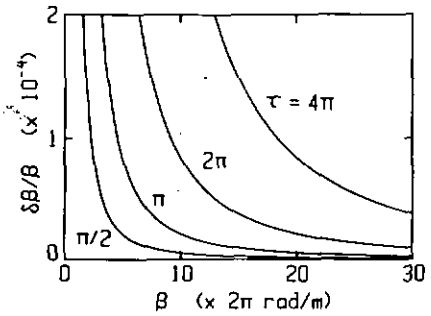

Fig. 2. Relative error $\delta\beta/\beta$ of the birefringence as a function of β for different twist rates τ (rad/m).

V. Sensitivity

The applied force is determined by measuring the phase difference between the two polarization modes,

$$\phi = (\beta_b - \beta_f)L = \pi ECLr^2/\lambda R^2 - 8CF/\lambda r, \quad (9)$$

where L is the fiber length. The phase difference due to the transverse force [second term in Eq. (9)] is independent of both the length of the fiber and the distribution of the force along the fiber (i.e., the effect is integrated over the fiber length). However, in a practical sensor configuration, the length of the fiber determines the maximum force supported by the sensing plate. The bending-induced phase difference [first term in Eq. (9)] depends only on the fiber configuration. It introduces a bias value to ϕ but does not change the sensitivity to the lateral force given by

$$d\phi/dF = -8C/\lambda r. \quad (10)$$

The sensitivity depends on the outer diameter $2r$ of the fiber. Therefore, in a configuration where the force is applied at different positions of the sensing plate, variations of the diameter along the fiber may cause sensitivity fluctuations. For a typical diameter of $2r = 126$ μm and for $\lambda = 820$ nm, the theoretical value of the sensitivity is found to be $d\phi/dF = 0.57$ rad/N. Furthermore, the stability of the sensor depends on the wavelength stability of the source and on the temperature dependence of the stress-optic coefficient, which has the value of 0.013%/°C.[11]

The sensitivity of the sensor can be increased by using a modified configuration where the force acts more than once on the same fiber. An example is illustrated in Fig. 3, where a fiber is pressed between four parallel plates, thus increasing the sensitivity by a factor of 3.

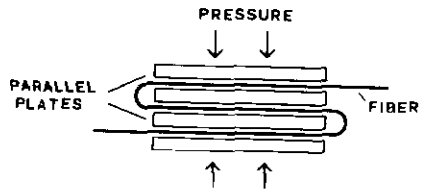

Fig. 3. Sensor configuration with increased sensitivity by a factor of 3.

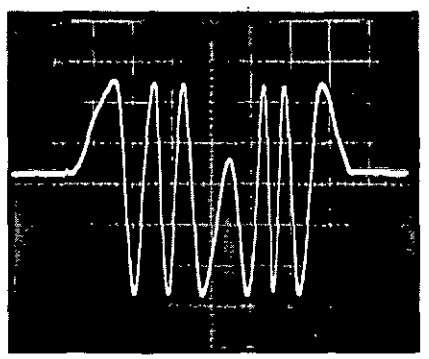

Fig. 4. Detector output vs time (0.1 s/div) for loading and unloading the sensor with ~3 kg.

VI. Experiment

An experimental arrangement consisting of a fiber loop with 4.5-cm radius of curvature pressed between two glass plates has been investigated. The plates are 15 mm thick and have standard window-glass flatness. The top plate (10 × 10 cm) is fixed to a rigid bottom plate (15 × 15 cm) by means of two parallel suspension Cu-Be bars which protect them against sideway displacements, while the force to be measured remains unperturbed. Sideway displacements of the top plate may twist the fiber resulting in optical activity which may modify the response of the output signals I_1 and I_2 [see Eq. (8) and Fig. 2]. An uncoated fiber of 126-μm diameter (LT-F0808C) exhibiting low intrinsic birefringence (<10°/m) and a power stabilized laser diode (CQL-13A) operating at 820 nm have been employed. The phase difference between the two propagating modes due to the bend is −0.57 rad, and the phase difference induced by the weight of the top plate (384 g) is 2.15 rad. Transparent adhesive tape at the input and output ends of the fiber was used to strip off eventual leaky modes guided by the fiber. Calibrated weights were used to test the sensor. The electronic phase measuring system, equipped with 12-bit A/D converters, was able to resolve an incremental load of 0.2 g (~1 mrad). The maximum load applied was 30 kg, which is ~1 kg/cm of fiber length. The sensitivity measured at the center of the plate was 5.50 rad/kg (or 0.56 rad/N). At the border of the plate, the observed relative sensitivity variations were <1%.

Figure 4 shows one of the detector signals (I_1 or I_2) as a function of time obtained by manually pressing and releasing the sensing plate with a force corresponding to ~3 kg. The resolution and stability of the sensor are

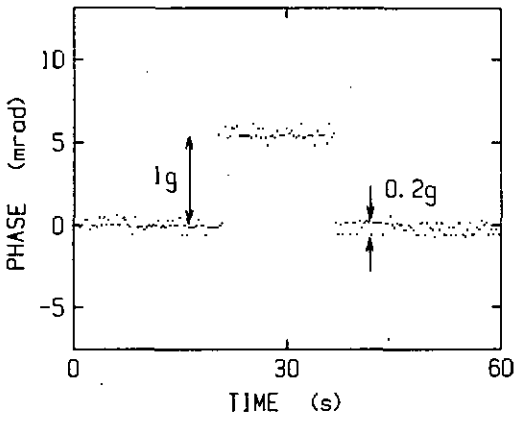

Fig. 5. Measured phase vs time for loading and unloading of 1-g wt. (Three measurements/s, 20-μs sample acquisition time).

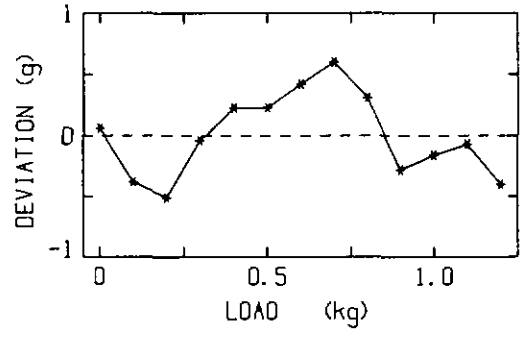

Fig. 6. Induced birefringence as a function of applied load. Deviation from linear least-square fit over the range of one period (2π rad or 1.14 kg).

illustrated in Fig. 5, where measurement of the loading and unloading of a weight of 1 g is shown as a function of time. The deviation from linearity between applied and measured load, starting from the zero bias load over a range corresponding to one period (1.14 kg or 2π rad), is shown in Fig. 6. The deviation was found to be <0.05% and is highly reproducible. At larger bias loads, similar deviations from linearity have been observed in intervals corresponding to one period each. However, the accuracy of the measurements decreased because of the increased inertial mass which makes the sensor more sensitive to mechanical vibrations and acoustic waves. Loading and unloading the sensor with 30 kg are reproducible to 1 part in 10^4, the limit being probably imposed by the mechanical reproducibility of the sensor.

VIII. Discussion and Conclusions

For increasing birefringence, the optical path length difference between the two propagating modes increases. Depending on the spectral composition of the light source, this may reduce the degree of polarization (or fringe visibility) at the output end of the fiber.[12] In the reported experiment, a laser diode operating in several longitudinal modes (about five modes with 0.3-nm mode spacing) has been employed. Therefore, for a birefringence corresponding to an applied load of 30 kg, a reduction of the degree of polarization of 4% is expected. This reduction, which appears as a common variation of the modulation depths of the signals I_1 and I_2, has been verified experimentally. It is worth noticing that the measuring system is insensitive to small common variations of the modulation depths, which do not change the ratio m_1/m_2 in Eq. (3). No special care has been taken to cut the endfaces at a specific angle to the fiber axis. However, the spectral width of the individual laser modes (~0.02 nm) is sufficiently large to avoid Fabry-Perot behavior of the sensor element.[13]

In conclusion: the possibility of using an all single-mode fiber polarimetric sensor configuration to measure static force or pressure with high resolution and accuracy has been investigated. We believe that the mechanical and geometrical properties of present low-birefringence single-mode fibers are good enough to enable force measurements with resolutions better than 1 part in 10^4 and over a wide dynamic range. For practical applications, however, technical problems concerning the construction of the sensing element remain.

References

1. Y. Namihira, M. Kudo, and Y. Mushiaka, "Effect of Mechanical Stress on the Transmission Characteristics of Optical Fibers," Trans. IECE Jpn. 60-C, 107 (1977).
2. M. Johnson, "In-line Fiber-Optical Polarization Transformer," Appl. Opt. 18, 1288 (1979).
3. N. Chinone and R. Ulrich, "Elasto-optic Polarization Measurement in Optical Fiber," Opt. Lett. 6, 16 (1981).
4. S. C. Rashleigh, "Acoustic Sensing with a Single Coiled Monomode Fiber," Opt. Lett. 5, 392 (1980).
5. J. Fields, C. Asawa, O. Ramer, and M. Barnoski, "Fiber Optic Pressure Sensor," J. Acoust. Soc. Am. 67, 816 (1980).
6. W. B. Spillman, "Multimode Fiber-Optic Pressure Sensor Based on the Photoelastic Effect," Opt. Lett. 7, 388 (1982).
7. A. Bertholds and R. Dändliker, "Microprocessor Based Phase Determination for High Resolution Optical Sensors," Electron. Lett. 21, 65 (1985).
8. R. Ulrich, S. C. Rashleigh, and W. Eickhoff, "Bending-Induced Birefringence in Single-Mode Fibers," Opt. Lett. 5, 273 (1980).
9. R. Ulrich and A. Simon, "Polarization Optics in Twisted Single-Mode Fibers," Appl. Opt. 18, 2241 (1979).
10. A. Barlow, D. Payne, M. Hadley, and R. Mansfield, "Production of Single-Mode Fibers with Negligible Intrinsic Birefringence and Polarization Mode Dispersion," Electron. Lett. 17, 725 (1981).
11. A. Barlow and D. Payne, "The Stress-Optic Effect in Optical Fibers," IEEE J. Quantum Electron. QE-19, 834 (1983).
12. S. C. Rashleigh, "Origins and Control of Polarization Effects in Single-Mode Fibers," IEEE, J. Lightwave Technol. LT-1, 312 (1983).
13. R. Ulrich and S. C. Rashleigh, "Beam-to-Fiber Coupling with Low Standing Wave Ratio," Appl. Opt. 19, 2453 (1980).

DEFORMATION OF SINGLE-MODE OPTICAL FIBERS UNDER STATIC LONGITUDINAL STRESS *

A. Bertholds and R. Dändliker
Institute of Microtechnology, University of Neuchatel
CH-2000 Neuchatel, Switzerland

Abstract

The deformation of single-mode fibers resulting from a longitudinally applied static force has been measured experimentally by means of high resolution heterodyne interferometry and analysed theoretically using second-order theory of elasticity and the photoelastic effect. Both the elongation of the fiber and the phase change of light propagating through the fiber have been measured as a function of tensile force. The values of the elastic constants measured for fibers with pure silica core and B_2O_3 doped cladding are $E = 6.41 \times 10^{10}$ N/m^2 for the Young's modulus, $\delta = -4.0$ for the nonlinearity constant of the longitudinal strain and $\beta = -2.3$ for the nonlinearity constant of the transverse strain. For unit elongations up to 0.3 %, no creep, hysterisis or relaxation effects have been observed within a resolution of one part in 10^4.

* Accepted for publication in IEEE Journ. of Lightwave Techn., 1987.

DEFORMATION OF SINGLE-MODE OPTICAL FIBERS UNDER STATIC LONGITUDINAL STRESS

Abstract

The deformation of single-mode fibers resulting from a longitudinally applied static force has been measured experimentally by means of high resolution heterodyne interferometry and analysed theoretically using second-order theory of elasticity and the photoelastic effect. Both the elongation of the fiber and the phase change of light propagating through the fiber have been measured as a function of tensile force. The values of the elastic constants measured for fibers with pure silica core and B_2O_3 doped cladding are $E = 6.41 \times 10^{10}$ N/m^2 for the Young's modulus, $\delta = -4.0$ for the nonlinearity constant of the longitudinal strain and $\beta = -2.3$ for the nonlinearity constant of the transverse strain. For unit elongations up to 0.3 %, no creep, hysterisis or relaxation effects have been observed within a resolution of one part in 10^4.

1. INTRODUCTION

When a static tensile force is applied to a single-mode optical fiber, nonlinear effects in the relation between stress and strain are observed in both the longitudinal and transverse direction [1]. Several papers report on the nonlinearity between strain and stress of fused silica fibers (not optical) under tension [2,3]. However, little is known about the second-order deformation of silica optical fibers under static longitudinal stress, and more generally, about the nonlinearity in the transverse strain (or Poisson's contraction) of fused silica.

In this paper, the deformation of silica single-mode fibers resulting from a longitudinally applied static stress is measured experimentally by means of high resolution heterodyne interferometry and analysed theoretically using second-order theory of elasticity for an isotropic material under finite deformation [4] and the photoelastic effect [5]. The experimental results obtained for silica optical fibers are compared with previously reported results obtained for silica fibers [2,3] and sinusoidally strained optical fibers [6].

First, the longitudinal strain is analysed by measuring interferometrically the elongation of a fiber as a function of an applied tensile force. Thereafter, the transverse (or radial) strain is investigated by measuring the phase change of light propagating through the fiber induced by the same tensile force. This second measurement allows to determine the nonlinearity of the transverse strain since, due to the photoelastic effect, both the longitudinal and transverse strain contribute to the optical phase change [1]. Both measurements are performed using the same experimental setup, the same fiber, the same phase measuring system, and under identical experimental conditions. The setup consists of a heterodyne Mach-Zehnder interferometer and an arrangement which allows to stress the fiber longitudinally by means of calibrated weights.

The deviation from linear theory (Hooke's law) of the deformation of optical fibers is of interest whenever large strains are involved. Examples are the analysis of crack-growth in fibers, tensile proof tests, installation of underwater optical cables and some fiber-optic sensor applications [7]. Hopefully, the results presented here may also be useful to a better understanding of the structure of silica glasses.

2. THEORY

2.1 Second-order theory of elasticity

Second order theory of elasticity predicts for a fiber of isotropic material under finite deformation by simple tension (no shear stress) a nonlinear relation between the applied stress and the resulting longitudinal and transverse strains [4], namely

$$\varepsilon_\ell = \varepsilon_0 + \delta\varepsilon_0^2 \,, \tag{1}$$

$$\varepsilon_t = -\nu\varepsilon_0 + \beta\varepsilon_0^2 \,, \tag{2}$$

where ε_0 denotes the applied stress σ_0 divided by the Young's modulus E, ν is the Poisson's ratio, and δ and β are two nonlinearity constants. The stress σ_0 is defined as the applied force per unit area of the unstrained fiber, so that

$$\varepsilon_0 = \sigma_0/E = F/\pi r^2 E \,, \tag{3}$$

where F is the tensile force and r the initial radius of the fiber. The strain tensor S_j is then given, in standard contracted form, by [4]

$$S_j = \begin{bmatrix} \varepsilon_t + \nu^2\varepsilon_0^2/2 \\ \varepsilon_t + \nu^2\varepsilon_0^2/2 \\ \varepsilon_\ell + \varepsilon_0^2/2 \\ 0 \\ 0 \\ 0 \end{bmatrix} \quad . \tag{4}$$

Thus, for a fiber under simple tension, the deformation is characterized by the Young's modulus, the Poisson's ratio, and the constants δ and β of the fiber material. The relation between these four parameters and the five fundamental elastical constants of an isotropic material is described in Ref.4.

The nonlinear behaviour of the longitudinal strain, as described by Eq.(1), can be explained by assuming a nonlinearity of the Young's modulus defined as

$$E' = d\sigma/d\varepsilon_\ell = E(1 + \gamma\varepsilon_\ell) \quad , \tag{5}$$

where $\sigma = \sigma_0/(1 + \varepsilon_t)^2$ is the stress of the strained fiber ($(1 + \varepsilon_t)^2$ accounts for the Poisson's contraction of the fiber cross-section) and γ is the nonlinearity constant introduced in Ref.2. It can be showns that δ has two contributions, namely $\delta = 2\nu - \gamma/2$. The first one results from the contraction of the fiber cross-section and the second one is due to the nonlinearity of the Young's modulus. As it will be shown later, for fused silica fibers the two contributions have opposite signs and the second one is 10 times larger then the first one.

Similarly, the nonlinear behaviour of the transverse strain (see Eq.(2)) can be explained by assuming a nonlinearity of the Poisson's ratio. The transverse strain can be written as $\varepsilon_t = -\nu'\varepsilon_\ell$, where

$$\nu' = \nu(1 + \omega\varepsilon_\ell) \tag{6}$$

and ν is the Poisson's ratio of the unstrained fiber. The nonlinearity parameter of the transverse strain becomes then $\beta = -\nu(\delta + \omega)$.

It is worth noting that when fabricating silica single-mode fibers, small quantities of GeO_2 and B_2O_3 are usually added in order to increase and decrease the refractive index of the fiber material with respect to undoped SiO_2 (see Fig.4) [8]. Consequently, the effective elastical constants of the fiber material may be slightly different to those of pure fused silica. In practice, the differences are small, so that the fiber can be considered as a mechanically homogeneous medium.

2.2 Photoelastic effect

The photoelastic effect describes the relation between the mechanical strain and the resulting refractive index change in the material. In standard contracted notation, the effect is described by [5]

$$\Delta(1/n^2)_i = \sum_j p_{ij} S_j , \qquad i,j = 1,2, \ldots, 6. \tag{7}$$

where $\Delta(1/n^2)_i$ denotes the changes of the indicatrix, n is the refractive index, p_{ij} is the strain-optic tensor and S_j the strain tensor written in contracted notation. For an isotropic material, the strain-optic tensor has the form of

$$p_{ij} = \begin{bmatrix} p_{11} & p_{12} & p_{12} & 0 & 0 & 0 \\ p_{12} & p_{11} & p_{12} & 0 & 0 & 0 \\ p_{12} & p_{12} & p_{11} & 0 & 0 & 0 \\ 0 & 0 & 0 & p_{44} & 0 & 0 \\ 0 & 0 & 0 & 0 & p_{44} & 0 \\ 0 & 0 & 0 & 0 & 0 & p_{44} \end{bmatrix} , \tag{8}$$

where $p_{44} = (p_{11} - p_{12})/2$, p_{11} and p_{12} are the individual strain-optic coefficients. For fused silica the photoelastic effect is small, so that $\Delta(1/n^2)_i = - 2\Delta n_i/n^3$ can be assumed. Light propagating through a longitudinally strained single-mode fiber is polarized along the transverse directions (i = 1, 2) and sees therefore a change of the refractive index

$$\Delta n = - (n^3/2)\Delta(1/n^2)_{1,2} = - (n^3/2)[S_1(p_{11} + p_{12}) + S_3 p_{12}] , \tag{9}$$

where S_1 and S_3 are the first and third elements of the strain tensor as described by Eq.(4). Thus, Δn has contributions from both the longitudinal

strain ε_ℓ and the transverse strain ε_t, which appear in S_1 and S_3, respectively. The optical phase change $\Delta\phi$ of the transmitted light is then given by

$$\Delta\phi = kL(n\varepsilon_\ell + \Delta n) \quad , \tag{10}$$

where $k = 2\pi/\lambda$ denotes the free space wavenumber, λ is the wavelength, L the fiber length, ε_ℓ the longitudinal strain and Δn the refractive index change of the core region (Eq. (9)). From Eq.(10) one sees that the optical phase is modified due to variations in both the physical length of the fiber (first term) and the refractive index (second term). For fused silica, the second contribution has negative sign and is 5 times smaller than the first one. The influence due to a variation of the fiber diameter (waveguide geometry effect) is small and therefore neglected [9]. Finally, the relation between the phase change and ε_0 (which is proportional to the applied tensile force as given by Eq.(3)) is obtained by introducing Eqs.(1), (2) and (9) into (10), yielding

$$\Delta\phi = knL[A\varepsilon_0 + B\varepsilon_0^2] \quad , \tag{11}$$

$$\varepsilon_0 = F/\pi r^2 E \quad , \qquad A = 1 - (n^2/2)[p_{12} - \nu(p_{11} + p_{12})] \quad ,$$

$$B = [1 - (n^2/2)p_{12}]\delta - (n^2/2)(p_{11} + p_{12})\beta - (n^2/4)[p_{11} + \nu^2(p_{11} + p_{12})] \quad ,$$

where δ and β are the two nonlinearity constants. Note that the phase change per unit fiber elongation described by the linear theory of elasticity ($B = 0$) is given by $(\Delta\phi/\Delta L)_{lin.} = knA$, where $\Delta L = \varepsilon_0 L$ denotes the fiber elongation.

To determine experimentally the four parameters which characterize the deformation of the fiber, it is necessary to measure first the longitudinal strain ε_ℓ as a function of the applied tensile force F. The Young's modulus E and the constant δ are then determined from the linear and quadratic terms in Eq.(1). Once the values of E and δ are known, the Poisson's ratio ν and the constant β can be obtained by measuring the phase change $\Delta\phi$ as a function of the tensile force F. Similarly, the values of ν and β are determined from the linear and quadratic terms in Eq.(11). It is assumed that the material parameters p_{11}, p_{12} and n, the fiber geometry (length L and radius r) and the optical wavelength are known.

3. EXPERIMENTAL SETUP

The experimental setup consists of a Mach-Zehnder interferometer (Fig.1), having in one arm an arrangement which allows to stress a fiber longitudinally by means of calibrated weights (Fig.2). The setup has two modes of operation, namely one where the two interferometer beams propagate through air and one where they propagate through fibers. The first configuration serves to measure the fiber elongation whereas the second one serves to measure the phase change of light propagating through the stressed fiber.

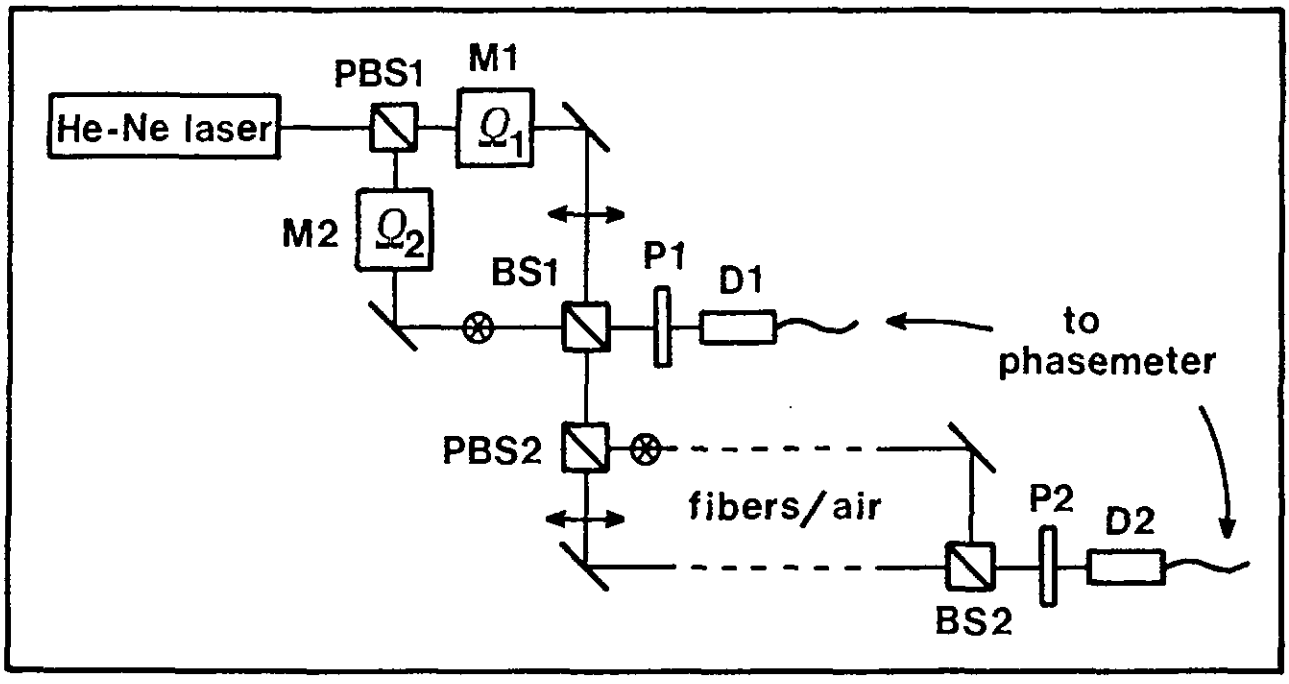

Fig.1. Heterodyne Mach-Zehnder interferometer (BS: beam splitter, M: acousto-optical modulator, PBS: polarizing beam splitter, P: polarizer, D: detector).

The heterodyne Mach-Zehnder interferometer employed for the measurements is illustrated in Fig.1. Light from a He-Ne laser (2 mW, linearly polarized) is split into two beams having equal intensities and orthogonal polarizations (horizontal and vertical) by means of a polarizing beam-splitter (PBS1). The beams pass each through an acousto-optical modulator (M1 and M2) and are then recombined in a beam-splitter (BS1). The driving frequencies of these modulators are Ω_1 = 40.1 MHz and Ω_2 = 40 MHz, so that the resulting beat frequency is $\Omega_1 - \Omega_2$ = 100 kHz. A photodetector (D1) behind a polarizer (P1), aligned at 45° with respect to the polarization directions, produces the reference signal $U_r = 1 + \sin[\Omega_1 - \Omega_2]t$. A second polarizing beam-splitter (PBS2) is employed to

separate the two beams of orthogonal polarization and different frequency into the two arms of the Mach-Zehnder interferometer. The two beams are recombined again by BS2 to produce the output signal $U_s = 1 + \sin[(\Omega_1 - \Omega_2)t + \phi]$, where ϕ is the optical phase difference between the two interferometer arms. The two sinusoidal electrical signals U_r and U_s are fed to a phasemeter and a fringe counter [10].

The arrangement used for the elongation of the fiber is shown schematically in Figs.2a and 2b. The fiber is stressed longitudinally by means of calibrated weights via a T-shaped construction which is guided vertically by means of four cantilever blades. The suspension (which is similar to the parallel guiding used in precision scales) protects the T-shaped construction against sideway displacements. For vertical displacements, however, it introduces a small force proportional to the displacement (or fiber elongation) due to the spring effect of the cantilever blades. To eliminate this effect, the suspension is attached to a vertical translation stage so that each time the fiber is stressed, the suspension is lowered by an amount equal to the resulting fiber elongation. The translation stage is controlled by a stepping motor with a resolution of 0.1 µm.

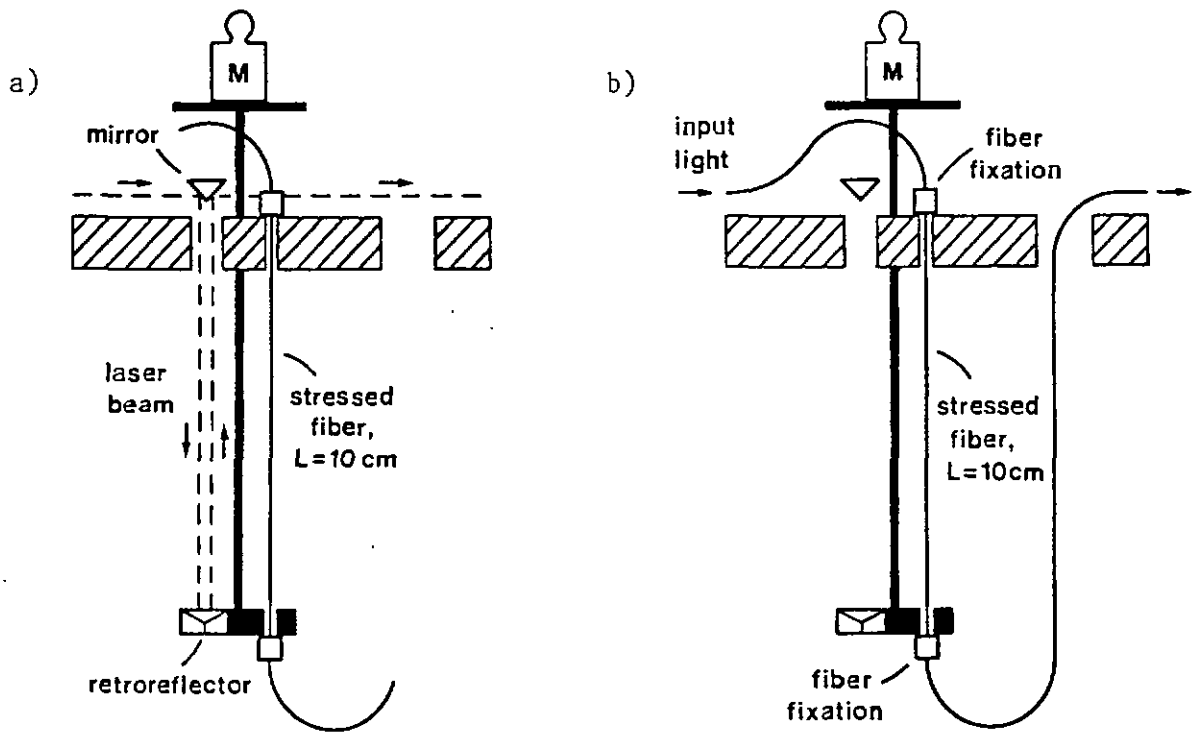

Fig.2. Arrangement for measuring the elongated fibers: a) configuration used for the measurement of the fiber elongation, b) configuration used for the measurement of the phase change of light propagating through the fiber.

The bare fibers, which have an outer diameter of about 125 µm, are stressed over a length of 10 cm. They are fixed mechanically by clamping between two flat aluminum surfaces over a length of 4 mm. The fibers are deliberately embedded in the aluminum by the clamping force in order to increase the contact surface and reduce the force-induced linear birefringence. Attemps have been made to fix the fibers by means of epoxy, however, the measurements were perturbed by slow deformations and creeping effects of the epoxy. The bare fibers are mounted carefully without introducing mechanical twist and are bent in planes either parallel or perpendicular to the direction of the linearly polarized light in order to avoid fading of the output signal. For the same reason, the direction of the lateral clamping force at the fiber fixations is aligned parallel to the direction of the linearly polarized light.

The stablilty and reproducibility of the fiber fixation as well as the elastic properties of the fiber material are demonstrated in Fig.3. The deformation of a fiber due to loading and unloading of 100 g weight is shown as a function of time. In this case, the phase fluctuations of the measuring system were $\pm 7^{\circ}$ (± 5 mg), which corresponds to a resolution of the applied load of one part in 10^4. Note that, within this resolution, no creep, hysterisis or relaxation effects are observed.

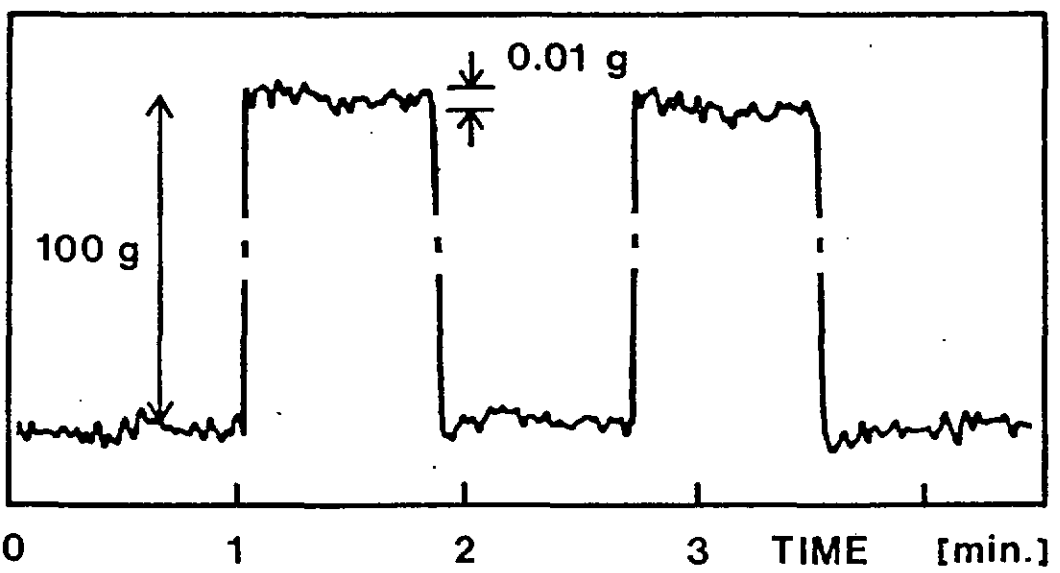

Fig.3. Fiber elongation measurement: loading and unloading of 100 g weight vs. time.

The two modes of operation of the elongation arrangement are shown in Figs.2a and 2b. For the measurement of the fiber elongation, one of the interferometer beams is deflected to a retroreflector fixed at the end of the elongated fiber (Fig.2a). In this case, the two interferometer beams propagate through air and the optical phase difference $\Delta\phi_\ell$ is proportional to the elongation ΔL, viz. $\Delta\phi_\ell = 2k\Delta L$, where $k = 2\pi/\lambda$. For the measurement of the phase change of light propagating through the fiber (Fig.2b), the two beams of the interferometer are launched into fibers, having approximatively the same length. The elongation of one of the fibers induces the phase difference which is described by Eq.(10).

The employed heterodyne measuring system has a phase accuracy of 1°. For the extension measurements, this corresponds to a fiber elongation of 0.9 nm or to an applied weight of 0.8 mg. During the measurements, the phase fluctuations due to temperature variations, mechanical vibrations and laser phase instabilities were in general smaller than $\pm 10^\circ$ and the long-term drift less than 5°/min. The fluctuations are somewhat higher when the beams propagate through fibers. They depend also on the optical path length missmatch of the interferometer arms. In order to improve the stability, the interferometer was mounted on a granit optical table and was protected against air currents.

4. EXPERIMENTAL RESULTS

Uncoated fused silica fibers (LT-F1506B) with an outer diameter of about 125 µm were used for the measurements. The refractive index profile of the fiber is shown in Fig.4. The cutoff wavelength is 500 nm and the core-cladding index difference 0.3 %. The core is made of pure SiO_2 and the inner and outer

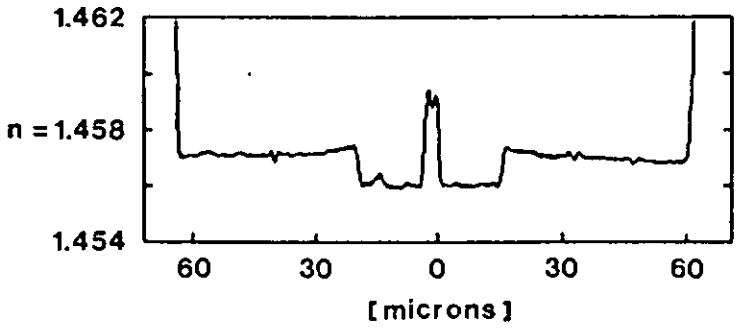

Fig.4. Refractive index profile of the investigated fiber (LT-F1506B). (measured by A. Witschi, R & D Group of the Swiss PTT)

claddings are doped with B_2O_3 (~10 % and 5 % respectively). The fibers are stressed over a length of 10 cm. The diameter variations over the sample length were measured to be less than ± 0.3 µm. The intrinsic linear birefringence of the fiber was smaller than 10 °/m.

The elongation of the fiber as a function of the applied tensile force is determined by differential measurements using calibrated weights. The force F is related to the applied weight M by F = Mg, where g is the gravity constant. The sensitivity, specified as the elongation induced by an additional weight of 20 g, is measured for different bias loads ranging from 75 g to 275 g. The minimum applied load is imposed by the weight of the loading support and the maximum load, which corresponds to a unit elongation of 0.3 % or an applied load per unit area of 24 kg/mm^2, is determined essentially by the risk of breaking the fiber.

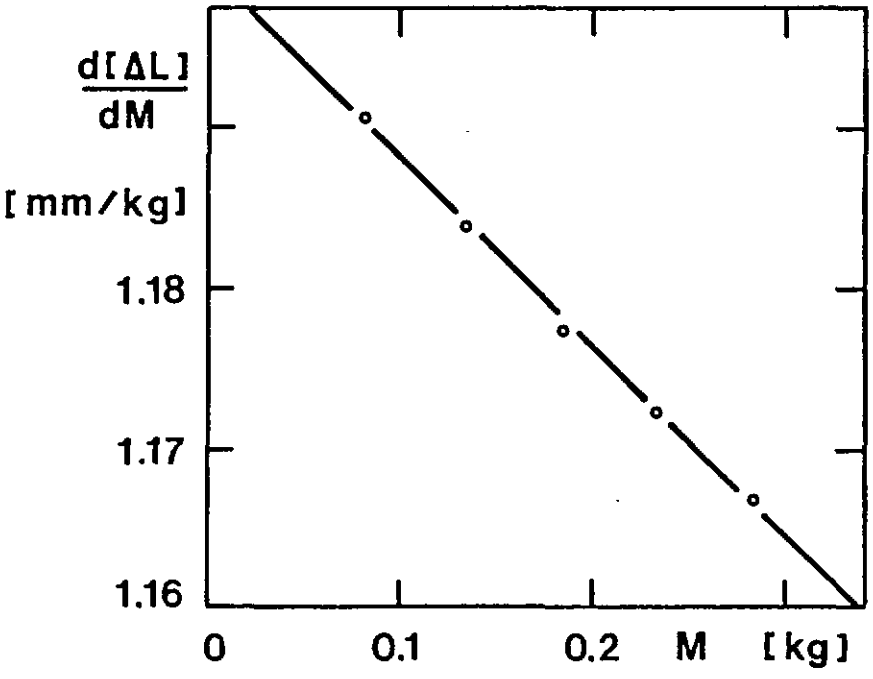

Fig.5. Measured sensitivity d(ΔL/dM) vs. bias load M (LT-F1506B).

A typical result is shown in Fig.5, where a linear decrease of the sensitivity d(ΔL)/dM is observed. By integrating the straight line fitted to the experimental points, the elongation ΔL of the fiber as a function of the applied load M is obtained as

$$\Delta L = \varepsilon_\ell L = aM - (b/2)M^2 \quad , \tag{12}$$

where a = 1.201 ± 0.002 mm/kg and b = 0.121 ± 0.002 mm/kg^2 in this particular case (fiber no.1 in Tab.1). The variations of a (0.2 %) and b (2 %) are comparable to the estimated experimental error.

Once the extension of the fiber as a function of the applied load is measured, the same procedure is carried out under identical experimental conditions (i.e., same fiber, same setup, same weights and same room temperature) but with the interferometer beams propagating through the fibers (Fig.2b). As before, the phase change as a function of the applied load is again determined by differential measurements. The result is shown in Fig.6, where again a linear decrease of the sensitivity $d(\Delta\phi)/dM$, specified now as the change of $\Delta\phi$ induced by an additional weight of 20 g, is observed. By integrating the straight line fitted to the points, $\Delta\phi$ is obtained as a function of the applied load M as

$$\Delta\phi = a'M - (b'/2)M^2 \quad , \tag{13}$$

with $a' = 13795 \pm 10$ rad/kg and $b' = 940 \pm 9$ rad/kg^2 in this particular case (fiber no.1 in Tab.1).

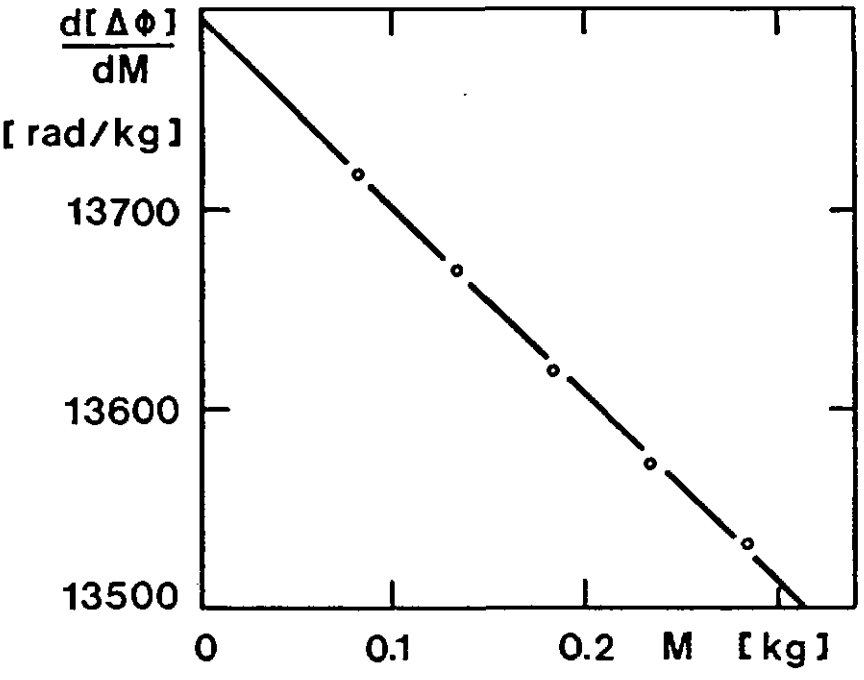

Fig.6. Measured sensitivity $d(\Delta\phi)/dM$ vs. bias load M (LT-B1506B).

The value of the Young's modulus is obtained by comparing the linear terms of Eqs.(1) and (12), yielding

$$E = gL/\pi r^2 a \quad , \tag{14}$$

where $g = 9.81$ m/s^2 is the gravity constant, L and r being the length and radius of the unstrained fiber, respectively. The nonlinearity constant δ is determined by comparing the quadratic terms in Eqs.(1) and (12). Using Eq.(14),

one gets $\delta = bL/2a^2$. Finally, the constant β is obtained by comparing the quadratic terms of Eqs.(11) and (13).

The results obtained for five different fiber samples are summarized in Tab.1. All the measured samples have the same length, namely L = 100.2 mm. The fiber diameters were measured individually with a resolution of 0.1 µm. The error of the diameters reported in Tab.1 is ± 0.3 µm. This corresponds to the maximum diameter variation or ellipticity of the fiber cross-section along the sample length. The mean value and the standard deviation of E is (6.41 ± 0.02) x 10^{10} N/m^2. This value is about 10 % lower than the Young's modulus of pure silica (SiO_2) measured in bulk, probably due to the presence of dopants in the fiber [11]. The mean value of the nonlinearity constant δ is $\delta = -4.0 \pm 0.2$, the standard deviation being about twice the experimental error. The value obtained for δ is somewhat higher than the previously reported values of -3.0 ± 0.9 [2] and - 2.4 ± 0.7 [3]. The former was measured on silica fibers having outer diameters of ~30 µm and the latter on fibers having diameters of ~4 µm. The higher value measured for optical fibers having diameters of ~125 µm can be explained by the fact that δ increases with the diameter of the sample, as observed in Ref.3. Note that the highly circular cross-section and precise diameter of optical fibers [8] allow to determine δ with high accuracy.

fiber no.	diameter [µm]	E [10^{10}N/m²]	δ	β
1	127.3	6.43	- 4.2	- 2.4
2	122.5	6.42	- 3.8	- 1.7
3	127.4	6.39	- 4.2	- 2.7
4	128.6	6.43	- 3.8	-
5	129.9	6.39	- 4.2	-
mean ± st. dev.		6.41±0.02	- 4.0±0.2	- 2.3±0.5

Tab.1. Summary of results for fused silica optical fibers (LT-F1506B).

The phase change per unit fiber elongation described by linear theory is given by $(\Delta\phi/\Delta L)_{lin.} = a'/a$ (see Eqs.(12) and (13)). Further, according to Eq.(11), $(\Delta\phi/\Delta L)_{lin.} = knA$, where A is a function of ν, p_{11} and p_{12}. Consequently, the

Poisson's ratio of the fiber material can be determined, provided that the values of the strain-optic coefficients p_{11} and p_{12} are known. When using the coefficients of bulk silica $p_{11} = 0.121$ and $p_{12} = 0.27$ [12], values for ν around 0.2 are obtained for all samples. This values are higher than the accepted values for SiO_2, which are between 0.16 and 0.17. Unfortunately, this difference can not be explained by the presence of B_2O_3 in the fiber, since the addition of B_2O_3 decreases slightly the Poisson's ratio compared to that of undoped SiO_2 [11]. Thus the strain-optic coefficients of the fiber material are presumably different from those of bulk silica. For this reason, the experimental measurement of the ratio a'/a was used to determine the effective values of the strain-optic coefficients rather than the Poisson's ratio of the fiber material. The method used to determine the individual strain-optic coefficients in a single-mode fiber is described in Ref.13. It consists of measuring, for the same fiber, both the phase change per unit fiber elongation and the optical activity per unit twist rate.

Finally, the mean value of the nonlinearity constant β of three measured samples (samples no.4 and 5 in Tab.1 are missing due to fiber breakage at the fixation) is $\beta = -2.3 \pm 0.5$. The material parameters $p_{11} = 0.113$, $p_{12} = 0.252$, $\nu = 0.16$ [13] and $n = 1.458$ have been used to calculate β. Although no value of the constant β is available for comparison, it is possible to compare our measurements with the results reported in Ref.6. In this experiment, the refractive index change of a sinusoidally stretched optical fiber was investigated. The nonlinear effects in the relation between the refractive index and the strain are described by a parameter D which, written in our notation, is given by $D = (\delta + 0.5)p_{12} + (\beta + 0.5\nu^2)(p_{11} + p_{12})$. Introducing our experimental values, we obtain $D = -1.7$, whereas Ref.6 measured $D = -1.0$. The difference is probably due to the dependence of the nonlinearity constants on the diameter of the strained fiber (fibers with smaller diameters were used in Ref.6) and to the fact that the fibers may have been doped differently.

5. CONCLUSIONS

An interferometric technique for measuring second-order deformations of single-mode optical fibers under static longitudinal stress has been described. It is based on the measurement of the elongation of the fiber and the phase change of light propagating through the fiber, both as a function of tensile force. The

deformation of a silica optical fiber has been measured experimentally and analysed theoretically using second-order theory of elasticity for an isotropic material under finite deformation and the photoelastic effect. For a fiber with pure silica core and B_2O_3 doped cladding, the Young's modulus of the unstrained fiber has been measurured to be $E = 6.41 \times 10^{10}$ N/m^2. The nonlinearity constants of the longitudinal and transverse strains have been measured to be $\delta = -4.0$ and $\beta = -2.3$ respectively. These nonlinearities can be explained by assuming a Young's modulus and a Poisson's ratio of the fiber material which depend on the longitudinal strain ε_ℓ in the following way: $E' = E(1 + 7.4\varepsilon_\ell)$, $\nu' = \nu(1 + 18\varepsilon_\ell)$, where E and ν are the Young's modulus and the Poisson's ratio of the unstrained fiber, respectively. For unit elongations up to 0.3 %, no creep, hysterisis or relaxation effects have been observed within a resolution of one part in 10^4.

6. REFERENCES

1. A. Bertholds and R. Dändliker, "Interferometric investigation of monomode fibers under longitudinal stress", Proc. 2nd Conf. on Opical Fiber Sensors (VDE-Verlag, Berlin, 1984), pp. 365-368.

2. F. Mallinder and B. Proctor, "Elastic constants of fused silica as a function of large tensile strain", Phys. and Chem. of Glasses, vol. 5, pp. 91-103, 1964.

3. B. Powell and M. Skove, "Measurement of higher-order elastic constants, using finite deformations", Physical Rev., vol .174, pp. 977-983, 1968.

4. F. Murnaghan, "Finite deformation of an elastic solid", (Wiley & Sons, New York, 1951), pp. 61-118.

5. J. Nye, "Physical properties of crystals", (Clarendon Press, Oxford, 1967), pp. 243-257.

6. M. Slonecker, D. Stowe, V. Tekippe and J. Beasley, "Effect of strain on light propagation in a single-mode optical fiber", Advances in Ceramics, vol. 2, pp. 209-218, 1980.

7. T. Giallorenzi, J. Bucaro, A. Dandridge, J. Siegel, J. Cole, S. Rashleigh and R. Priest, "Optical fiber sensor technology", IEEE Journ. of Quantum Electr., vol. QE-18, pp. 626-665, 1982.

8. S. Miller and A. Chynoweth, "Optical fiber telecommunications", (Academic Press, INC., New York, 1979), pp. 167-258.

9. G. Hocker, "Fiber-optic sensing of pressure and temperature", Appl. Opt., vol. 18, pp. 1445-1448, 1979.

10. J. Mastner and V. Masek, "Electronic instrumentation for heterodyne holographic interferometry", Rev. Sci. Instrum, vol. 51, pp. 926-931, 1980.

11. N. Lagakos and J. Bucaro, "Pressure desensitation of optical fibers", Appl. Opt., vol. 20, pp. 2716-2720, 1981.

12. W. Primak and D. Post, "Photoelastic constants of vitreous silica and its elastic coefficient of refractive index", Journ. of Appl. Physics, vol. 30, pp. 779-788, 1959.

13. A. Bertholds and R. Dändliker, "Determination of the individual strain-optic coefficients in single-mode optical fibers", to be published in IEEE Journ. of Lightwave Techn.

DETERMINATION OF THE INDIVIDUAL STRAIN-OPTIC COEFFICIENTS IN SINGLE-MODE OPTICAL FIBERS *

A. Bertholds and R. Dändliker
Institute of Microtechnology, University of Neuchatel
CH-2000 Neuchatel, Switzerland

Abstract

A method to determine the individual strain-optic coefficients in single-mode fibers is described. It is based on two photoelastic experiments, namely the polarimetric measurement of optical activity induced by mechanical twist and the interferometric measurement of optical path length change induced by static longitudinal strain. For fibers with pure silica core and B_2O_3 doped cladding, the optical activity per unit twist rate and the phase change per unit fiber elongation have been measured to be $g = 0.1472$ and $\Delta\phi/\Delta L = 1.150 \times 10^7$ rad/m, respectively. The strain-optic coefficients have been measured to be $p_{11} = 0.113$ and $p_{12} = 0.252$. These values are 7 % lower than those of bulk silica.

* Accepted for publication in IEEE Journ. of Lightwave Technology.

DETERMINATION OF THE INDIVIDUAL STRAIN-OPTIC COEFFICIENTS IN SINGLE-MODE OPTICAL FIBERS

Abstract

A method to determine the individual strain-optic coefficients in single-mode fibers is described. It is based on two photoelastic experiments, namely the polarimetric measurement of optical activity induced by mechanical twist and the interferometric measurement of optical path length change induced by static longitudinal strain. For fibers with pure silica core and B_2O_3 doped cladding, the optical activity per unit twist rate and the phase change per unit fiber elongation have been measured to be $g = 0.1472$ and $\Delta\phi/\Delta L = 1.150 \times 10^7$ rad/m, respectively. The strain-optic coefficients have been measured to be $p_{11} = 0.113$ and $p_{12} = 0.252$. These values are 7 % lower than those of bulk silica.

1. INTRODUCTION

The polarization properties of single-mode optical fibers intended for telecommunication and sensor applications [1-2] are more or less sensitive to any kind of mechanical perturbation because of the photoelastic effect [3]. The photoelastic effect which relates the change of refractive index to the mechanical strain is, for an isotropic material, described by the two strain-optic coefficients p_{11} and p_{12} [4]. In general, when calculating the influence of mechanical perturbations such as elongation, lateral and hydrostatic compression, torsion and bending of optical fibers, the values of the strain-optic coefficients measured for bulk fused silica are employed [5]. However, due to the presence of doping elements in the core (usually GeO_2) and/or in the inner and outer claddings (usually B_2O_3), and considering that light transmitted by a fiber propagates partially in the inner cladding, the effective values for fibers may be different from those for bulk silica. So far, for optical fibers only the value of $(p_{11} - p_{12})$, obtained by measuring the optical activity induced by mechanical twist, have been reported in the literature [6-8]. The reported experimental results suggest significant

difference between the strain-optic coefficients for optical fibers and for bulk silica. However, to the best of our knowledge, no attempt has yet been made to measure the individual coefficients directly in a fiber.

In the present paper, a method to determine the individual strain-optic coefficients in single-mode fibers is described. The difference between the two strain-optic coefficients ($p_{11} - p_{12}$) is obtained by measuring the twist induced optical activity [6], whereas their individual values are obtained by measuring interferometrically the phase change of light propagating through the fiber induced by static longitudinal strain [9,10]. An attempt to determine the Poisson's ratio of the fiber material by measuring the bend-induced birefringence [8,11] is also reported.

2. DETERMINATION OF p_{11} AND p_{12}

When a fiber is twisted, optical activity is introduced due to the torsional strain induced in the core region [6]. The induced activity α is proportional to the twist rate, namely

$$\alpha = g\tau \,, \tag{1}$$

where τ is the mechanical twist per unit fiber length and g is a material parameter given by

$$g = -(n^2/2)(p_{11} - p_{12}) = -n^2 p_{44} \,, \tag{2}$$

where n is the refractive index of the core region. In the absence of linear birefringence, the effect of a twisted fiber is to rotate linearly polarized light at a rate of $\alpha/2$ per unit fiber length. Thus, the parameter g can be measured accurately by launching linearly polarized light into a fiber and by measuring at the output the twist-induced polarization rotation. Then, from the experimental value of g and using Eq.(2), the difference between the strain-optic coefficients ($p_{11} - p_{12}$) can be obtained directly [6].

By measuring the phase change of light propagating through the fiber due to a longitudinal strain, it is possible to determine the individual values of the two coefficients p_{11} and p_{12}. Using first order theory of elasticity and the photoelastic effect, and assuming that the fiber is elastic and mechanically

homogeneous, the phase change $\Delta\phi$ induced by an elongation ΔL is given by [9]

$$\Delta\phi = k[n\Delta L + \Delta n L] = kn\Delta L\{1 - (n^2/2)[p_{12} - \nu(p_{11} + p_{12})]\} \quad , \tag{3}$$

where $k = 2\pi/\lambda$ denotes the free space wavenumber, λ is the wavelength, n the refractive index, Δn the refractive index change and ν the Poisson's ratio of the fiber material. From Eq.(3) one sees that the optical phase is modified due to changes in both the physical length of the fiber (first term) and the refractive index (second term). For fused silica, this second contribution has negative sign and is 5 times smaller than the first one. The influence due to a change in the fiber diameter (waveguide geometry effect) is small and can therefore be neglected [9].

Thus, from the experimentally measured values of g and $\Delta\phi/\Delta L$, and provided that the Poisson's ratio is known, the strain-optic coefficients p_{11} and p_{12} can be obtained using Eqs.(2) and (3). The Poisson's ratio ν can be determined experimentally by measuring the linear birefringence induced in a fiber by bending. The bend-induced birefringence β_b is given by [11]

$$\beta_b = - \pi n g(1 + \nu) r^2/\lambda R^2 \quad , \tag{4}$$

where g is the material parameter defined in Eq.(2), r the radius of the fiber and R the radius of curvature. When a fiber is bent, birefringence is introduced due to both an asymmetrical transverse stress distribution induced in the core region (photoelastic effect, Eq.(4)) and a modification of the fiber geometry (waveguide geometry effect). Recently, it has been demonstrated that the contribution from the waveguide geometry effect is 400 times smaller and therefore neglegible [12].

3. EXPERIMENTS AND RESULTS

Uncoated fused silica fibers (LT-F1506B) with an outer diameter of about 125 µm were used for the measurements. The refractive index profile of the fiber is shown in Fig.1. The cutoff wavelength is 500 nm and the core-cladding index difference 0.3 %. The core is made of pure SiO_2 and the inner and outer claddings are doped with B_2O_3 (~10 % and 5 % respectively). It is worth noting here that, for a wavelength of 633 nm, about 30 % of the light intensity guided by the fiber propagates in the inner cladding. The intrinsic linear birefrin-

gence of the fiber was measured to be less than 10°/m and the intrisic circular birefringence smaller than 5°/m. It was found that the diameter of the fiber shows fast variation of 0.2 µm with a periodicity of ~ 0.2 m superimposed on slow variations of the order of several microns over a length of more than 2 m. The fiber-samples used in the experiments were all taken from a single 20 m piece of fiber.

The optical activity per unit twist rate is determined experimentally by launching linearly polarized light from a He-Ne laser (λ = 633 nm)) into the fiber and by measuring the rotation of the emerging polarization as a function of the mechanical twist. The fiber is uncoated and positioned straight on a flat surface. Both ends are fixed using small drops of epoxy. The epoxy serves also to strip off the leaky cladding modes. Five different samples with individual lengths of 1 m have been measured at room temperature for mechanical twists up to 20 turns. The mean value and the standard deviation of the optical activity per unit twist rate are g = 0.1472 ± 0.0004. The deviation of ~ 0.3 % is comparable to the estimated experimental error. Note that g is determined very accurately and that its value does not seem to vary substantially between different samples of the same fiber type. The obtained value of g can be compared with the experimental values reported by other authors, namely 0.13 [6], 0.138 [8] and 0.146 [13] (all measured for λ = 633 nm), and with the value of 0.158, calculated from Eq.(2) with the parameters n = 1.458, p_{11} = 0.121 and p_{12} = 0.27 for pure bulk silica [5]. It is interesting to see that the values for fibers are 7 % to 18 % lower than the expected value for bulk silica. These differences can be explained by the presence of dopants (Ge, B) in the core and/or in the cladding which modify the photoelastic properties of the fiber material. Furthermore, the effective value of g may also depend on the refractive index profile of the fiber which, for a given wavelength, determines the ratio of light intensities guided in the core and in the cladding.

The phase change $\Delta\phi$ of light propagating through the fiber caused by the elongation ΔL is determined accurately using a heterodyne Mach-Zehnder interferometer (λ = 633 nm) and an arrangement which allows to stress the fiber longitudinally by means of calibrated weights [10]. The results obtained for three different samples are summarized in Tab.1. The mean value and the standard deviation of the phase change per unit fiber elongation are $\Delta\phi/\Delta L = (1.150 \pm 0.002) \times 10^7$ rad/m. The deviation is comparable to the estimated experimental error. The obtained value can be compared with the

previously reported value of 1.20×10^7 rad/m [9] and the expected value of 1.13×10^7 rad/m, calculated with the parameters for bulk silica.

To determine the individual values of p_{11} and p_{12}, it is necessary to know the Poisson's ratio ν of the fiber material (see Eq.(3)). An attempt to determine ν by measuring the bend-induced birefringence as a function of the radius of curvature is described in the following. Figure 2 shows the experimental setup used for the measurements. Linearly polarized light from a He-Ne laser is launched into a circularly bent fiber at 45° with respect to the bending axis, thus exciting the two polarization modes with equal intensity. At the output end, the bend-induced phase difference between the two modes is measured using a Soleil-Babinet compensator (SBC) and a polarizer, aligned perpendicular to the direction of the linearly polarized input light. The fiber is uncoated and bent in a single loop on a flat surface. Two glass capillaries having an inner diameter of 130 µm, an outer diameter of 1 mm and a length of 10 mm are used to hold the fiber in a circular loop (see Fig.2). Bending radii ranging from 15 mm to 50 mm are realized by displacing the output end of the fiber which is attached to the measuring arrangement. The bend-induced phase difference is given by $\phi_b = \beta_b L$, where β_b is the induced birefringence (see Eq.(4)) and L the length of the bent fiber. The experiment consists therefore in measuring the phase difference as a function of the radius of curvature, obtained by measuring the linear displacement of the detection arrangement. A summary of the results obtained for three different samples is given in Tab.2. The mean value and standard deviation of the constant $\phi_b R/r^2$ (r is the radius of the fiber) is $(7.73 \pm 0.11) \times 10^6$ rad/m. The standard deviation of ± 1.5 % is mainly due to the error of the measured fiber diameter and the variations of this diameter. The value of $\phi_b R$ is determined with an accuracy of better that 0.5 %. The obtained value of $\phi_b R/r^2$ can be compared with the previously reported value of 8.13×10^6 rad/m [8] and the expected value of 8.34×10^6 rad/m, calculated with the parameters for bulk silica.

Using Eq.(4) with n = 1.458 and the experimentally determined values of g and $\phi_b R/r^2$, one gets $(1 + \nu) = 1.154 \pm 0.018$ which yields for the Poisson's ratio itself $\nu = 0.154 \pm 0.018$. Although $(1 + \nu)$ has been experimentally determined with an accuracy of 2 %, the value of ν remains uncertain within about 10 %. Nevertheless, the obtained result is in good agreement with the values for bulk silica reported in the litterature, which are between 0.16 and 0.17. Considering that for optical fibers with B_2O_3 doped cladding the effective value of

ν may be expected to be slightly lower [14], it is reasonable to assume for the investigated fiber a Poisson's ratio of $\nu = 0.16$, with an error of ± 0.01.

4. DISCUSSION AND CONCLUSION

From the experimental measurements of the optical activity per unit twist rate g and the optical phase change per unit fiber elongation $\Delta\phi/\Delta L$, and assuming a Poisson's ratio of $\nu = 0.16 \pm 0.01$, the values of the individual strain-optic coefficients are determined (using Eqs.(2) and (3)) to be $p_{11} = 0.113 \pm 0.005$ and $p_{12} = 0.252 \pm 0.005$. The errors of p_{11} (5 %) and p_{12} (2 %) are essentially due to the uncertainty of ν.

The obtained results are compared in Tab.3 with values measured previously by Primak & Post [5] and Borelli & Miller [15] for bulk silica. The former used a static interferometric technique, whereas the latter employed an ultrasonic method. Usually, the values reported by Primak & Post are utilized because of their higher accuracy (2 %).

The wavelength dependence of $p_{44} = (p_{11} - p_{12})/2$ has been investigated by measuring the optical activity per unit twist rate $g = -n^2 p_{44}$ for two different wavelengths, using a He-Ne laser (633 nm) and a GaAs laser diode (880 nm) respectively. The measured wavelength dependence of g is $dg/d\lambda = 0.013\ \mu m^{-1}$. This value is somewhat higher than the previously reported value of $0.009\ \mu m^{-1}$ [7]. The relative wavelength dependence of p_{44} is given by

$$(1/p_{44})(dp_{44}/d\lambda) = (1/g)(dg/d\lambda) - (1/n)(dn/d\lambda) \quad . \qquad [5]$$

Using $dn/d\lambda = 0.011\ \mu m^{-1}$ [7], the relative dependence of p_{44} is 8.0 % μm^{-1}. Note that although the values shown in Tab.3 were measured at different wavelengths, the dispersion is so small that the difference is within the experimental error.

In conclusion, a method to determine the effective individual strain-optic coefficients p_{11} and p_{12} in single-mode fibers has been described. The optical activity induced by mechanical twist, the phase change of light propagating through the fiber induced by static longitudidinal strain and bend-induced birefringence have been measured experimentally with high accuracy. For all three experiments, the standard deviation of the values measured for different

samples of the same fiber were comparable to the estimated experimental error. For a fiber with a pure silica core and a cladding doped with B_2O_3 (LT-F1506B), the material parameter g and the strain-optic coefficients have been measured to be g = 0.1472, p_{11} = 0.113 and p_{12} = 0.252, respectively. These values are 7 % lower than those of bulk silica. The obtained results, together with the values of g reported in the litterature, suggest that the effective strain-optic coefficents in optical fibers are somewhat lower than those of bulk silica. This is probably due to the presence of dopants in the fiber material. Furthermore, the effective values may also depend on the refractive index profile of the fiber which, for a given wavelength, determines the ratio of light intensities guided in the core and in the cladding.

5. REFERENCES

1. D. Payne, A. Barlow and J. R. Hansen, "Development of low- and high birefringence optical fibers", IEEE Journ. of Quantum Electr., vol. QE-18, pp. 477-488, 1982.

2. T. Giallorenzi, J. Bucaro, A. Dandridge, J. Siegel, J. Cole, S. Rashleigh and R. Priest, "Optical fiber sensor technology", IEEE Journ. of Quantum Electr., vol. QE-18, pp. 626-665, 1982.

3. S. Rashleigh, "Origins and control of polarization effects in single-mode fibers", Journ. of Lightwave Tech., vol LT-1, pp. 312-331, 1983.

4. J. Nye, "Physical properties of crystals", (Clarendon Press, Oxford, 1967) pp. 243-257.

5. W. Primak and D. Post, "Photoelastic constants of vitreous silica and its elastic coefficient of refractive index", Journ. of Appl. Physics, vol .30, pp. 779-788, 1959.

6. R. Ulrich and A. Simon, "Polarization optics in twisted single-mode fibers", Appl.Opt., vol. 18, pp. 2241-2251, 1979.

7. A. Barlow and D. Payne, "The stress-optic effect in optical fibers", IEEE Journ. of Quantum Electr., vol. QE-19, pp. 834-839, 1983.

8. A. Smith, "Birefringence induced by bends and twists in single-mode optical fiber", Appl. Opt., vol. 19, pp. 2606-2611, 1980.

9. C. Butter and G. Hocker, "Fiber optics strain gauge", Appl. Opt., vol. 17, pp. 2867-2869, 1978.

10. A. Bertholds and R. Dändliker, "Deformation of single-mode optical fibers under static longitudinal stress", IEEE Journ. of Lightwave Techn, Special Issue on Fiber-Optic Sensors, ...

11. R. Ulrich, S. Rashleigh and W. Eickhoff, "Bending-induced birefringence in single-mode fibers", Opt. Lett., vol. 5, pp. 273-275, 1980.

12. X. Fang and Z. Lin, "Birefringence in curved single-mode optical fibers due to waveguide geometry effect - Perturbation analysis", IEEE Journ. of Lightwave Tech., vol. LT-3, pp. 789-794, 1985.

13. A. Barlow, J. Hansen and D. Payne, "Birefringence and polarization-mode dispersion in spun single-mode fibers", Appl. Opt., vol. 20, pp. 2962-2968, 1981.

14. N. Lagakos and J. Bucaro, "Pressure desensitation of optical fibers", Appl. Opt., vol. 20, pp. 2716-2720, 1981.

15. N. Borelli and R. Miller, "Determination of the individual strain-optic coefficients of glass by an ultrasinic technique", Appl. Opt., vol. 7, pp. 745-750, 1968.

6. FIGURES

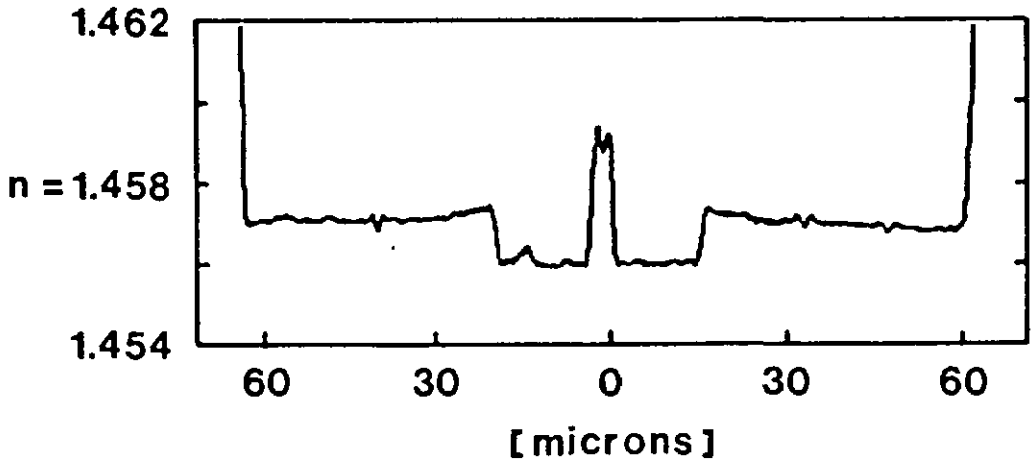

Fig.1. Refractive index profile of the investigated fiber (LT-F1506B). (measured by A. Witschi, R & D Group of the Swiss PTT)

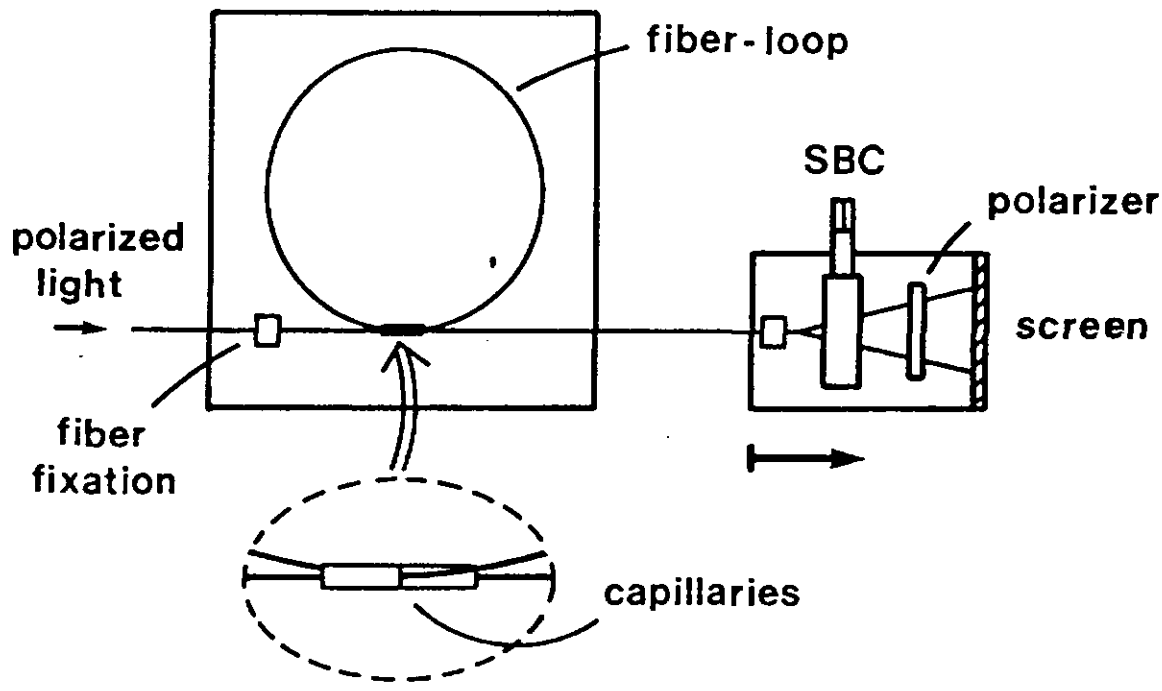

Fig.2. Experimental setup used to measure the bend-induced birefringence.

Tab.1. Summary of the experimental results for the phase change per unit fiber elongation.

fiber no.	length [mm]	diameter [μm]	$\Delta\Phi/\Delta L$ [rad/m]
1	100.2	122.6	1.152×10^7
2	100.2	127.3	1.149×10^7
3	100.2	127.4	1.150×10^7
mean ± st. dev.			$(1.150 \pm 0.002) \times 10^7$

Tab.2. Summary of the experimental results for the bend-induced birefringence.

fiber no.	diameter 2r [μm]	$\phi_b R/r^2$ [rad/m]
1	121.3 ± 0.3	7.66×10^6
2	122.6 ± 0.4	7.67×10^6
3	123.2 ± 0.3	7.85×10^6
mean ± st. dev.		$(7.73 \pm 0.11) \times 10^6$

	sample	λ [μm]	p_{11}	p_{12}
Primak & Post [5]	bulk silica	589	0.121	0.27
Borelli & Miller [17]	bulk silica	633	0.126	0.26
present work	silica fiber	633	0.113	0.252

Tab.3. Comparison of experimental values for the strain-optic coefficients.